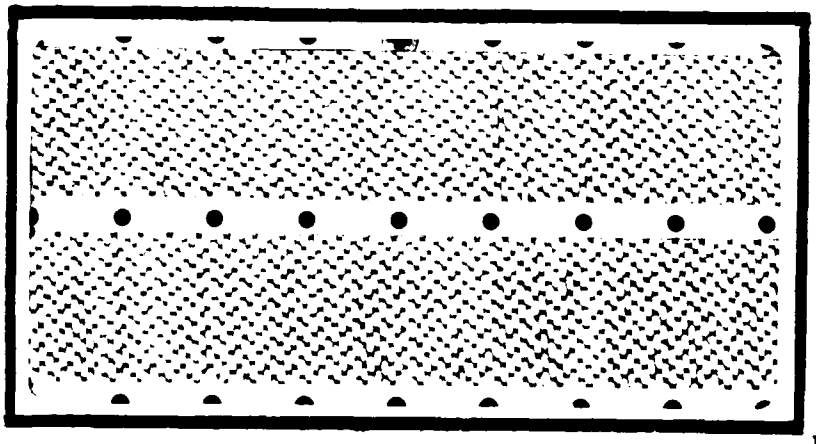

DEPARTMENT OF THE AIR FORCE

AIR UNIVERSITY

AIR FORCE INSTITUTE OF TECHNOLOGY

Wright-Patterson Air Force Base, Ohio

AFIT/GAE/AA/88M-2

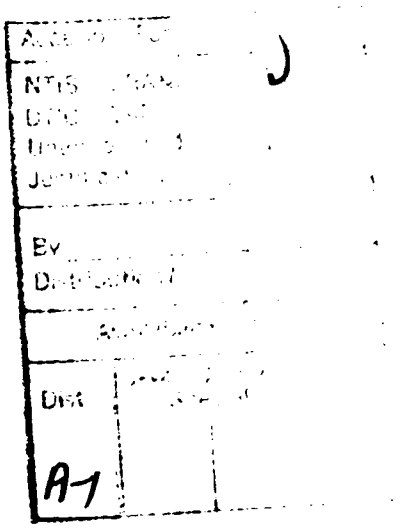

INVESTIGATION OF BOUNDARY LAYER DISTURBANCES CAUSED BY PERIODIC HEATING OF A THIN RIBBON

THESIS

Brenda Haven
Captain, USAF

AFIT/GAE/AA/88M-2

AFIT/GAE/AA/88M-2

INVESTIGATION OF BOUNDARY LAYER DISTURBANCES CAUSED BY PERIODIC HEATING OF A THIN RIBBON

THESIS

Presented to the Faculty of the School of Engineering

of the Air Force Institute of Technology

Air University

In Partial Fulfillment of the

Requirements for the Degree of

Master of Science in Aeronautical Engineering

Brenda Haven, B.S.

Captain, USAF

March 1988

Preface

Controlling a laminar boundary layer by the mechanical vibration of a thin Nichrome ribbon provided a challenge greater than I had anticipated. The unpredictability of the ribbon response to a pulsed voltage input often led to discouragement, and then to a new idea, a new approach, another objective.

Several people provided primary assistance in this effort to uncover new results. Professor Mario Carbonaro, of the von Karman Institute for Fluid Dynamics, Brussels, Belgium, gave advice and arranged for technical support whenever I needed it. Mr. Nicholas Yardich, AFIT lab supervisor, and his assistants provided the necessary equipment and know-how to make the experiments work. Dr. Milton Franke, my advisor, was invaluable in helping to plan my course of action and always patient in his guidance of this project. Each of these and many others deserve a vote of thanks.

Finally, I would like to thank my husband Mark for his love and constant encouragement given during what must have seemed like a very long and arduous task.

Brenda Haven

This thesis was prepared on a Kaypro PC using "ChiWriter" by Horstmann Software Design Corporation. The printer was an Epson Spectrum LX-80.

Table of Contents

List of Figures

List of Tables

List of Symbols

Symbol		Units
A	Surface area	m^2
$A(x)$	Boundary Condition Amplitude	m/s
c	Specific heat of Nichrome	kJ/kgK
c_i	Temporal amplification rate	m/s
c_r	Phase velocity in x-direction	m/s
f	Frequency	Hz
h	Convective heat transfer coefficient	W/m^2K
k_f	Air conductivity at reference temp	W/mK
k_n	Conductivity of Nichrome I	W/mK
l	Length	m
m	Mass per unit length	kg/m
Nu_m	Mean Nusselt number	—
p	Instantaneous pressure	N/m^2
P	Mean pressure	N/m^2
p^+	Pressure fluctuation	N/m^2
q_s	Surface heat flux	W
q_v	Volume heat flux	W
Re_w	Reynolds number based on ribbon width	—
Re_{δ_1}	Reynolds number based on displacement thickness	—
s	Thickness of ribbon	mm
T	Temperature	K or C
t	Time	s
U	Mean velocity in x-direction	m/s
U_e	Mean velocity at boundary layer edge	m/s

U_∞	Mean free stream velocity	m/s
u	Instantaneous velocity in x-direction . . .	m/s
u_r	Local velocity over ribbon	m/s
u^+	Velocity fluctuation in x-direction	m/s
V	Voltage	V
v	Instantaneous velocity in y-direction . . .	m/s
v^+	Velocity fluctuation in y-direction	m/s
w	Width of ribbon	mm
x	Distance from leading edge	m
y	Distance above flat plate surface	mm
z	Transverse distance from plate centerline .	mm
$\mathcal{T}$	Tension	N
$\mathcal{V}$	Volume	m^3
υ	Displacement	m
α	Disturbance wavelength ($2\pi/\lambda$)	m^{-1}
β_i	Degree of amplification or damping	s^{-1}
β_r	Frequency of partial oscillation	s^{-1}
δ	Boundary layer thickness	mm
δ_1	Boundary layer displacement thickness . . .	mm
η	Similarity variable	—
λ	Disturbance wavelength	m
ν	Kinematic viscosity	m^2/s
ρ	Density	kg/m^3
τ	Time constant	s
ϕ	Stream function amplitude	m^2/s
ψ	Stream function	m^2/s
ω	Frequency	Hz

Subscripts

a	Anemometer
amb	Ambient condition
corr	Corrected value
exp	Experimental value
f	Reference condition
max	Maximum value
mean	Mean value
min	Minimum value
p	Paint and label values
r	Ribbon
tc	Thermocouple value
∘	Mean value

Abstract

Wind tunnel experiments were conducted to investigate the use of a periodically heated Nichrome ribbon as a boundary layer control device. The specific items of interest were: 1) the physical parameters governing the ribbon behavior, 2) the consequence of the ribbon on the downstream development of the laminar boundary layer, and 3) the controllability of the ribbon to produce the desired consequence.

The thin ribbon was placed on or near the surface of 0.76-m and 0.91-m-long, flat plate models. The periodic voltage applied across the ribbon caused it to vibrate at a frequency or frequencies harmonic with the input frequency. The amplitude and frequency composition of the vibration was influenced by input voltage and frequency, applied tension to the ribbon, and flow velocity over the model.

The disturbances detected in the boundary layer immediately downstream of the vibrating ribbon exhibited the same frequency characteristics as the ribbon. The evolution of these disturbances in the boundary layer was studied by positioning a hot wire anemometer, boundary layer probe at different locations behind the ribbon. The selective amplification and damping of the disturbance frequencies agreed with the predictions of linear Tollmien-Schlichting

stability theory.

The ribbon vibration could not be controlled to provide a specified vibration frequency or amplitude with the control system used in this research. Boundary layer control schemes requiring careful selection of a controlling disturbance would be extremely difficult to implement using this technique. Without precise control of the ribbon vibration, unwanted frequencies are introduced into the boundary layer. The interaction of these disturbances was shown to accelerate the laminar to turbulent transition process.

INVESTIGATION OF BOUNDARY LAYER DISTURBANCES CAUSED BY PERIODIC HEATING OF A THIN RIBBON

I. Introduction

Active boundary layer control has generated much interest because of the benifits that can be gained from controlling the laminar to turbulent transition point. Moving the transition point downstream often reduces the overall drag and heat transfer at the surface, whereas, moving the transition point forward may be useful in preventing boundary layer separation.

Several techniques which have shown great promise in the area of boundary layer control are: suction, blowing, and surface heating or cooling. Another technique, which is the topic of this thesis, is to control the generation and growth of the disturbances which lead to transition. The superposition of a carefully selected controlling disturbance has been successful in reducing the boundary layer disturbances which precede transition (6,13,14,19,24).

This thesis explores the possibility of generating a controlling disturbance through the excitation of a thin Nichrome ribbon. Kudelka (11) found that sinusoidal velocity disturbances could be generated in the boundary layer by applying a periodic voltage pulse to a ribbon mounted on the surface of a flat plate model.

Background

In an environment where external perturbations are small, laminar to turbulent transition begins with the growth of two-dimensional periodic disturbances or Tollmien-Schlichting (TS) waves. Schubauer and Skramstad (23:69-78) observed the natural development of these waves within a laminar boundary layer. To obtain quantitative information about the development of these waves, they introduced a two-dimensional artificial disturbance into the boundary layer. This single frequency disturbance was generated by a thin metal strip made to vibrate using a magnetic field and alternating current. They observed that the amplification rate, wavelength, amplitude, and phase velocity of the propagating waves were in agreement with the linear stability theory proposed years earlier. The subsequent growth and evolution of the TS disturbances were further studied by Klebanoff, et al. (9:1-31). Their experiments demonstrated the different stages in the progression from laminar to turbulent flow. This chain of events begins with the two-dimensional instability of the laminar boundary layer, or the appearance of the TS waves. These two-dimensional waves increase linearly in amplitude until three-dimensional instabilities appear. The non-linear interaction between the two-dimensional waves and the growing three-dimensional instabilities causes the formation of a longitudinal eddy system. Locally high regions of

vorticity, resulting from the peak-and-valley structure of the longitudinal eddy system, give rise to bursts of turbulence. This is followed by the formation of turbulent spots, and finally by the rapid coalescence of these spots into fully turbulent flow.

The eventual development of turbulence is linked to the amplitude of the TS waves. For sufficiently small amplitudes these waves exhibit linear, two-dimensional behavior. If the amplitude of the TS waves is allowed to increase freely, three-dimensional instabilities develop and interact with the existing two-dimensional TS waves. Many experiments have explored the possibility of delaying transition by prolonging the time between the initial formation of the TS waves and the appearance of the three-dimensional instabilities. This was done by injecting a controlling disturbance into the boundary layer which would cancel or reduce the growing TS instability waves.

The work of Thomas (24:233-250) used two electromagnetically excited ribbons (2.5-mm-long and 0.05-mm-thick) located 0.3 m and 0.6 m downstream of the leading edge of a flat plate and spaced 0.4 mm from the surface. A two-dimensional TS type disturbance was generated by the first wire. The second wire responded by forcing another disturbance of equal amplitude and antiphased to cancel the developing disturbances. This work showed that it is possible to delay transition by a wave-superposition scheme. However, the three-dimensional disturbances, which appeared

as a result of the interaction between the primary and background disturbances, remained in the flow. A conclusion obtained from this effort was that the control disturbance should be injected soon after the primary disturbance to minimize the formation of these non-linear three-dimensional disturbances.

A similar control technique was used by Gilev (7:243-248). In his experiments a vibrator was built into a flat plate, 0.49 m from the leading edge. The vibrater was activated using a magnetic field and alternating current. Just upstream, a metal ribbon was placed slightly above the surface. The vibration of this ribbon was induced by the same mechanism. A control scheme, using the ribbon to initiate the two-dimensional disturbance and the antiphased vibration of the vibrator to cancel it, resulted in successful wave subtraction.

Liepmann, Brown, and Nosenchuck (14:187-200), in water tunnel experiments, used periodic heating of thin surface films to produce boundary layer oscillations. The flush mounted heating films, or strips, were placed on the surface of a flat plate model, transverse to the free stream flow. The heating films were used because they offer potential advantages over the vibrating ribbon technique. These advantages include: 1) with no current, flow over the model remains undisturbed by the presence of the heaters; 2) the shape of the heating elements can be freely chosen; 3) they can be easily modulated both in time and spanwise

coordinates; and 4) the effect of heating is easier to represent in a theoretical study. The successful excitation of TS waves by periodic heating prompted follow-on water tunnel experiments by Liepmann and Nosenchuck (13:201-204). These experiments used a second heating element, downstream of the first, to either cancel or reinforce the initial disturbance. These experiments demonstrated the possibility of actively controlling transition using a superposition technique. Subsequent water tunnel experiments by Nosenchuck, Lynch, and Stratton (19:619-625) used longitudinally placed heating elements to delay transition by cancelling the three-dimensional disturbances in the flow. By careful actuation of several longitudinal heating elements, low-speed streaks were generated in the flow. These low-speed regions, which lead to transition, were then attenuated by a second array of heating elements. Results indicate that this technique of local surface heating can reduce the incidence of turbulent bursting through the weakening of the low-speed streaks.

Maestrello, et al., experimentally (17), numerically (2), and theoretically (18) investigated the use of similar heating elements in air. The experiments were performed using an elliptic airfoil. Thin Nichrome heating elements, embedded in a ceramic substrate, were placed flush with the surface of the airfoil. Periodic heating of the elements excited disturbances in the boundary layer. Sound was then used to control the development of these disturbances. The

experimental results showed that surface heating can be used to trigger single small amplitude or fully transitional disturbances. Also, the presence of a favorable pressure gradient increases the receptivity of the boundary layer to the heating excitation. The numerical approach related the temperature, velocity, and pressure disturbances to localized surface heating. This method was used to simulate the excitation of a controlling boundary layer disturbance which could be used to either cancel or reinforce the TS instability waves. General observations of the these approaches were that the influence of heating in air acts to destabilize the boundary layer, and that the coupling between temperature and viscosity is much weaker in air than in water. The overall results of the analyses and experiments indicate active heating may be an effective mechanism in controlling the laminar to turbulent transition point in air.

Gedney investigated a control scheme using sound to excite the TS waves, followed by the forced transverse vibration of the leading edge of the flat plate model. These experiments demonstrated that laminar boundary layer transition can be strongly influenced by a linear interaction between sound excitation and plate vibration (6:1158-1160;12:283-294).

Objective and Scope

Active control of a laminar boundary layer is contingent upon the ability to introduce disturbances of a prescribed nature. To delay transition, the created disturbances must by carefully controlled such that the amplitude and phase characteristics interact to reduce the growing instabilities in the boundary layer. The previously mentioned techniques of imparting a controlling disturbance are: 1) mechanical excitiation of a thin ribbon by means of a magnetic field and an alternating current, 2) periodic heating of transverse and longitudinal surface films, and 3) transverse vibration of the model leading edge. This thesis investigates the possibility of generating such a controlling disturbance through the vibration of a thin Nichrome ribbon when subjected to a periodic voltage pulse. This technique was first used by Kudelka (11) to generate TS type disturbances in the boundary layer over a flat plate.

The objective of this thesis was to investigate the use of this thin Nichrome ribbon as a boundary layer control device. To accomplish this, experiments were conducted to gain an understanding of: 1) the physical parameters which govern the ribbon vibration, 2) the immediate and downstream boundary layer response to the ribbon vibration, and 3) the effect of the ribbon temperature alone on boundary layer stability.

II. Theory

Ribbon Vibration

The behavior of the Nichrome ribbon is determined by the input in the form of an electrical pulse, the environment, and the physical properties of the ribbon material. Various Nichrome ribbons were made to vibrate by applying the pulsed voltage shown in Fig 1.

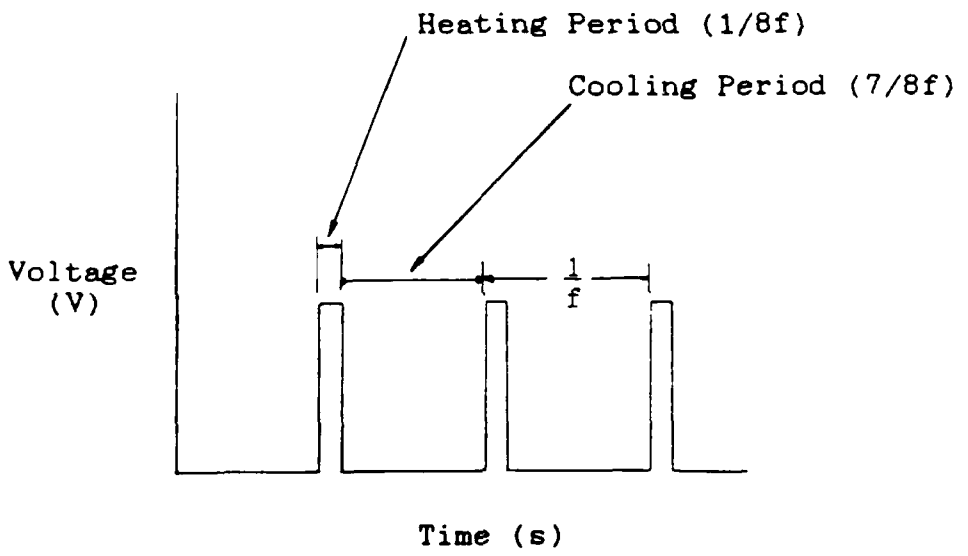

Fig 1. Voltage Input to Nichrome Ribbon.

The duration of the pulse remained constant throughout the experiments. The reasons for selecting a pulse time equal to one-eighth of the total cycle time were: 1) shorter pulse times result in a more concentrated and effective voltage for a given root-mean-square (rms) voltage, and 2) this was the shortest pulse which could be

produced by the function generator. The rms voltage is referred to in the experimental results. This quantity is related to the voltage of the pulse by the following equation:

$$V_{rms} = \left[\frac{1/8f}{1/f} (V_{pulse})^2 \right]^{1/2} \qquad (1)$$

The free vibration of the Nichrome ribbon can be qualitatively described using the one-dimensional wave equation:

$$\frac{\partial^2 v}{\partial t^2} = \frac{\mathcal{T}}{m} \frac{\partial^2 v}{\partial x^2} , \qquad (2)$$

where $\mathcal{T}$ is the tension and m is the mass per unit length of the ribbon (10:134-137).

The free vibration characteristics are given by the solution to this partial differential equation (10:117-123). Assuming the ends of the ribbon are fixed, the natural frequencies are integral multiples of $\pi(\mathcal{T}/ml^2)^{1/2}$. Since the length of the ribbon changes with temperature, these frequencies will be influenced by energy input to the ribbon (elongation) and convective cooling by the environment (contraction).

The characteristics of the ribbon vibration are determined by the ribbon natural frequencies and nature of the forcing function. The forcing mechanism arises from the periodic voltage input to the ribbon. The periodic voltage in Fig 1 can be written as an infinite series of sinusoidal components, or a Fourier series. The forcing function to

the ribbon becomes (25:347-348):

$$f(t) = V_{pulse}\left\{ \frac{1}{8} + \sum_{n=1}^{\infty} \frac{1}{\pi n} \left[\sin\left(\frac{\pi n}{4}\right) \cos(2\pi nft) + \sin(2\pi nft) - \cos\left(\frac{\pi n}{4}\right) \sin(2\pi nft) \right] \right\} \quad (3)$$

The predicted response of the ribbon is typically a multi-frequency vibration. However, when a frequency component of the input approaches one of the natural frequencies, a resonant condition is established. The resulting oscillations become large and have a single dominant frequency (10:134-137). This resonant behavior is influenced by anything that changes the natural frequencies of the ribbon. These parameters include ribbon tension; voltage input (heat addition); and heat loss through convection, conduction, radiation, etc.

Ribbon Heating and Time Constant

The heating and time constant characteristics of the Nichrome ribbon were investigated by modeling the ribbon as a thermally thin wall (8:4.37,38). This model assumes all heat received, given up, and generated by the body diffuses instantaneously throughout the material with no temperature gradients. The use of this model is contingent upon the Biot number Bi being less the 0.1:

$$Bi = \frac{h\ s}{k_n} = 9.6 \times 10^{-5} h, \qquad (4)$$

where s is the thickness and k_n is the conductance (20:2.36) of the Nichrome ribbon. The value of the convective heat transfer coefficient h in air is typically of the order 100 W/m^2K (3:393). Substitution of this value into eq (4) indicates that the thermally thin wall approximation is valid.

For a thermally thin wall, the instantaneous heat balance is written as:

$$q_s + q_v = \rho c \forall \frac{dT}{dt}, \qquad (5)$$

where q_s is the heat received or given up at the body surface; q_v is the heat internally generated by the body; and $\rho c \forall \frac{dT}{dt}$ is the rate of heat storage by the body.

For a single Nichrome ribbon suspended horizontally in free air, convective heat transfer is considered as the only means of heat transfer at the surface. Convective cooling of the ribbon is expressed as:

$$q_s = hA(T_{amb} - T). \qquad (6)$$

Substitution of eq (6) into eq (5) gives:

$$q_v + hA(T_{amb} - T) = \rho c \forall \frac{dT}{dt}. \qquad (7)$$

For uniform ribbon properties, ambient conditions, and

assuming the convective heat transfer coefficient to be constant with respect to time and temperature, eq (7) can be integrated to yield the following:

$$\frac{T - T_o}{T_{amb} - T_o + q_v/hA} = 1 - \exp\left(\frac{-hA}{\rho c \mathcal{V}} t\right), \qquad (8)$$

where T_o is the initial ribbon temperature.

The collection of terms, $\frac{\rho c \mathcal{V}}{hA}$, is considered to be the time constant of the system. This parameter is specified by the ribbon characteristics and the surrounding fluid environment. Table I gives a set of typical characteristics for the Nichrome ribbon.

Table I. Typical Characteristics of Nichrome Ribbon

Density ρ kg/m^3	Specific Heat c kJ/kgK	Width w mm	Thickness s mm	Length l m
8246*	0.448*	0.79	0.127	0.3

* Properties of Nichrome I (20:2.36).

For the above values, the time constant τ in seconds is 202/h, where h is measured in W/m^{2}K. The mean ribbon temperature can be approximated using an energy balance between the root-mean-square (rms) input voltage and the convective heat loss:

$$q_v = \frac{V_{rms}^2}{R} = hA(T_{mean} - T_{amb}). \qquad (9)$$

The value of h can be experimentally determined using eq (9) and the measured temperature rise for a given input.

The preceding analysis assumed convection to be the only dissipative mechanism. When the ribbon is mounted on the model and remains in contact with the surface, some of the energy used to raise the temperature of the ribbon is lost through conduction to the model surface. This would require an increase in the voltage input to the ribbon to obtain a specified ribbon temperature. However, as the ribbon expands during heating (even when in tension) it rises slightly above the surface. This reduces the heat loss through conduction. Rough estimates of the ribbon temperature and time constant were determined using eq (8) and an appropriate convective heat transfer coefficient h. The calculation of h as air is forced over the plate mounted ribbon was analytically determined using the model in Fig 2.

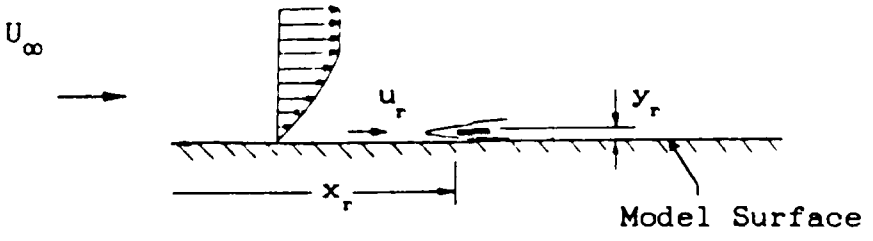

Fig 2. Model to Calculate h for a Surface Mounted Ribbon.

The ribbon lies a distance y_r above the surface of the model. The ribbon itself is treated like a flat plate, having a temperature T_{mean} and an approaching velocity u_r specified by the Blasius solution for the x_r and y_r location of the ribbon on the model. The properties of the air, subscripted with the letter f, are evaluated at a reference temperature: $T_f = (T_{mean} + T_{amb})/2$.

The convective heat transfer coefficient is obtained by calculating the mean Nusselt number, $Nu_m = \frac{h\ w}{k_f}$. For a flat plate Nu_m is given by (16:285-298):

$$Nu_m = \frac{h\ w}{k_f} = 0.664\ (Pr_f)^{1/3}(Re_{wf})^{1/2}. \qquad (10)$$

Equations (10) and (8) can be used to estimate the heating behavior of the ribbon.

Laminar Flow Stability Theory

Stability theory is primarily concerned with individual sine waves, or TS waves, propagating in the boundary layer parallel to the wall. The amplitude of these waves is sufficiently small to permit the use of linear stability theory.

The formulation of two-dimensional incompressible stability theory begins with the Navier Stokes equations written in Cartesian coordinates (16:3.3-5):

$$\frac{\partial u}{\partial t} + \frac{u\partial u}{\partial x} + \frac{v\partial u}{\partial y} + \frac{1\partial p}{\rho\partial x} = \nu\nabla^2 u \qquad (11a)$$

$$\frac{\partial v}{\partial t} + \frac{u\partial v}{\partial x} + \frac{v\partial v}{\partial y} + \frac{1\partial p}{\rho\partial y} = \nu\nabla^2 v \qquad (11b)$$

$$\frac{\partial u}{\partial x} + \frac{\partial v}{\partial y} = 0 \qquad (11c)$$

The resultant motion and pressure may be decomposed into steady parallel mean flow quantities, plus small superimposed non-steady disturbances:

$$u(x,y,t) = U(y) + u^+(x,y,t) \qquad (12a)$$

$$v(x,y,t) = v^+(x,y,t) \qquad (12b)$$

$$p(x,y,t) = P(x,y) + p^+(x,y,t) \qquad (12c)$$

Substituting the above quantities into eqs (11a,b,c); neglecting the quadratic terms in the fluctuating components; and subtracting the mean flow solution of eqs (11a,b,c); the equations in terms of the disturbance quantities u^+, v^+, and p^+, are written as:

$$\frac{\partial u^+}{\partial t} + U\frac{\partial u^+}{\partial x} + v^+\frac{dU}{\partial y} + \frac{1\partial p^+}{\rho\partial x} = \nu\nabla^2 u^+ \qquad (13a)$$

$$\frac{\partial v^+}{\partial t} + U\frac{\partial v^+}{\partial x} + \frac{1\partial p^+}{\rho\partial y} = \nu\nabla^2 v^+ \qquad (13b)$$

$$\frac{\partial u^+}{\partial x} + \frac{\partial v^+}{\partial y} = 0 \qquad (13c)$$

The stream function $\psi(x,y,t)$ satisfying eq (13c) represents a single oscillation of the disturbance:

$$\psi(x,y,t) = \phi(y)\ \exp\ [i(\alpha x - \beta t)] \qquad (14)$$

The velocity components of the disturbance are then given by:

$$u' = \frac{\partial \psi}{\partial y} = \phi'(y) \exp[i(\alpha x - \beta t)] \qquad (15a)$$

and

$$v' = -\frac{\partial \psi}{\partial x} = -i\phi(y) \exp[i(\alpha x - \beta t)] \qquad (15b)$$

In terms of temporal theory,

$\beta = \beta_r + i\beta_i$,

$\alpha = 2\pi/\lambda$,

and $c = \frac{\beta}{\alpha} = c_r + ic_i$,

where β_r represents the frequency of partial oscillation, β_i and c_i determine the degree of amplification or damping, λ is the wavelength of the disturbance, and c_r is the phase velocity of the wave in the x-direction.

Substitution of eqs (15a,b) into eqs (13a,b) gives the fundamental equation for the stability theory of laminar flows, referred to as the Orr-Sommerfeld equation:

$$(U - c)(\phi'' - \alpha^2\phi) - U''\phi = \frac{-i}{\alpha Re}(\phi'''' - 2\alpha^2\phi'' + \alpha^4\phi), \qquad (16)$$

where $Re = U_\infty \delta/\nu$ and differentiation is with respect to y/δ. Specifying the boundary conditions at $y = 0$:

$$u' = v' = 0 \;:\; \phi = 0 \;:\; \phi' = 0,$$

and at $y \to \infty$:

$$u' = v' = 0 \;:\; \phi = 0 \;:\; \phi' = 0,$$

the stability problem becomes an eigenvalue problem. For a

known flow velocity profile U(y), a specified mean flow Reynolds number Re, and a given disturbance wavelength λ, eq (16) will determine $\phi(y)$ and c. Setting the degree of amplification or damping to zero ($c_i = 0$), the curve of neutral stability can be developed for a two-dimensional incompressible boundary layer with two-dimensional disturbances (22:457-462).

The development of a two-dimensional TS disturbance is easily followed using this curve (Fig 3). The position of a disturbance in proximity to the region of instability is calculated from the location (Re_{δ_1}) and frequency characteristics ($2\pi f\delta_1/U_e$) of the disturbance. Disturbances lying inside this region are amplified, whereas, those outside the region are damped.

The transition from laminar to turbulent flow can be studied by tracing the growth of the two-dimensional TS disturbances as the boundary layer develops. As the two-dimensional disturbances pass through the instability region, the amplitude increases until the disturbance enters again into a region of stability, or its amplitude becomes sufficiently large to cause the formation of three-dimensional flow patterns.

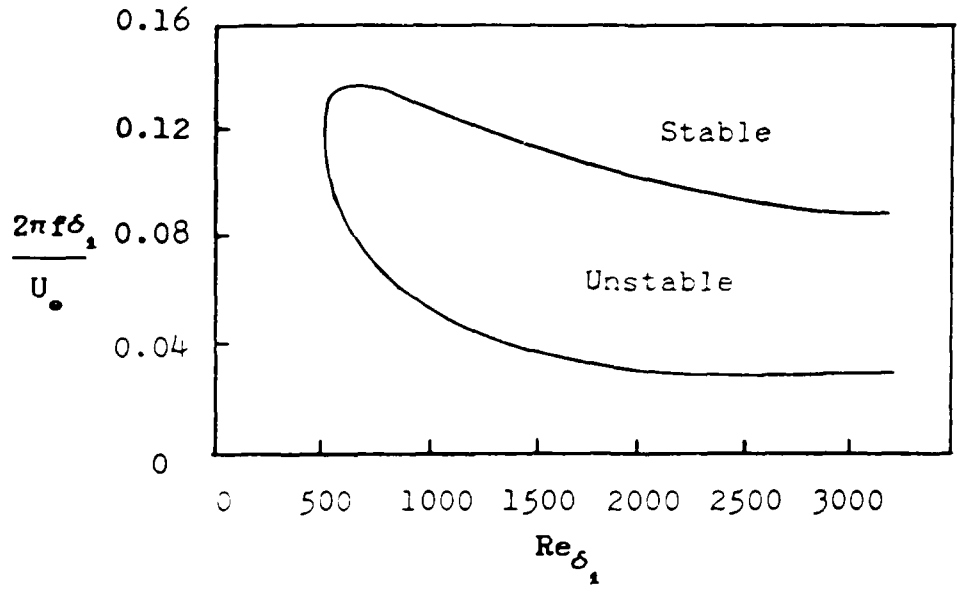

Fig 3. Curve of Neutral Stability for a Two-Dimensional Boundary Layer with Two-Dimensional Disturbances.

The above analysis deals with the free oscillations (TS waves) or normal modes of the laminar boundary layer. The problem investigated in this thesis contains forced oscillations due to a vibrating ribbon. To address the influence of these forced oscillations, the concept of receptivity is introduced.

> "By receptivity is meant the means by which a particular forced disturbance enters the boundary layer and the nature of its signature in the disturbance flow. If the initial disturbances are sufficiently large, they can grow by forcing mechanisms to non-linear levels and lead directly to turbulent flow. If they are small, they will tend to excite free disturbances in the boundary layer. These free disturbances are the aforementioned normal modes of the boundary layer and are often referred to as Tollmien-Schlichting (T-S) waves. The nature of each of these normal modes is determined from the solution of the eigenvalue problem arising from consideration of the linearized disturbance equation subject to appropriate boundary conditions." (21:1)

Unlike the linear stability problem, the receptivity phenomenon is not an eigenvalue problem because of non-homogeneous surface boundary condition. The vibrating ribbon represents an external forced oscillation or forcing disturbance. The 'neutral' solution to the linearized disturbance equations in this case specifies a boundary layer response having the same frequency as the forcing disturbance. The vibration of the ribbon may be simply modeled by the boundary condition:

$$v^*(x,0,t) = A(x)\cos\omega t, \qquad (17)$$

where A(x) is the disturbance amplitude and ω is the ribbon circular frequency (21:1-7). Gaster presents a solution in general terms to the above problem (5:433-441).

The previous analysis, based on linear stability theory, represents the first stage in the transition from a laminar to turbulent boundary layer. As the TS waves increase in amplitude, they begin to deviate from the predicted linear behavior. Three-dimensional instabilities appear and interact with the large two-dimensional waves. The flow patterns established by this interaction represent the second stage in the boundary layer development. Following this stage is an abrupt change in the character of the wave motion. Turbulent spots appear and rapidly coalesce to form a completely turbulent boundary layer.

External influences, such as free stream turbulence and the presence of longitudinal vortices on surfaces having

concave streamwise curvature (Taylor-Goertler vortices), accelerate the appearance of the second stage by prematurely introducing three-dimensional vortex structures into the boundary layer. The consequence of this interaction is to move the transition point of the boundary layer upstream (1:1-21).

III. Experimental Apparatus

The experiments of this thesis were performed in two separate wind tunnel facilities. Both facilities are open circuit, suction type wind tunnels. They provide low-speed, low-turbulence flow throughout the test section. The AFIT 9-Inch wind tunnel has a 9 by 9 by 36-in (0.239 by 0.239 by 0.9-m) test section with instrumentation access ports located every 127 mm along the centerline. The maximum flow velocity through the empty test section is 16.5 m/s. The turbulence level (u^{+}/U_{∞}) remains near 0.25 percent over the entire velocity range. The L-2A wind tunnel, at the von Karman Institute for Fluid Dynamics (VKI), has an octagonal test section 0.28-m wide and 1.3-m long. Modular plexiglass side panels allow for direct mounting of the model to the test section walls. The top of the test section is designed to allow for continuous transverse and longitudinal movement of the boundary layer traversing mechanism. The maximum flow velocity through the empty test section is 36 m/s. The turbulence level is 0.5 percent for flow velocities between 6 and 25 m/s. Further details of the wind tunnels are given in Appendices A and B.

The general equipment arrangements are shown in Figs 4, 5, and 6. Each apparatus consists of two basic systems. The first system provided the input in the form of an electrical pulse to the ribbon. This input was produced by a function generator and power amplifier, then monitored

using a digital voltmeter, frequency counter, and/or dual trace oscilloscope. The second system monitored the influence of the input on the physical response of the ribbon and/or the development of the boundary layer. The physical motion of the ribbon was monitored using a Fotonic (light) sensor. Ribbon heating was measured using thermocouples welded to the ribbons and temperature indicating paints and labels. The boundary layer development was monitored using a hot wire anemometer and boundary layer probe. The output of the Fotonic sensor and anemometer was observed with a low frequency spectrum analyzer, a dual trace oscilloscope, and a personal computer or x-y recorder. A detailed equipment description is given in Appendix C.

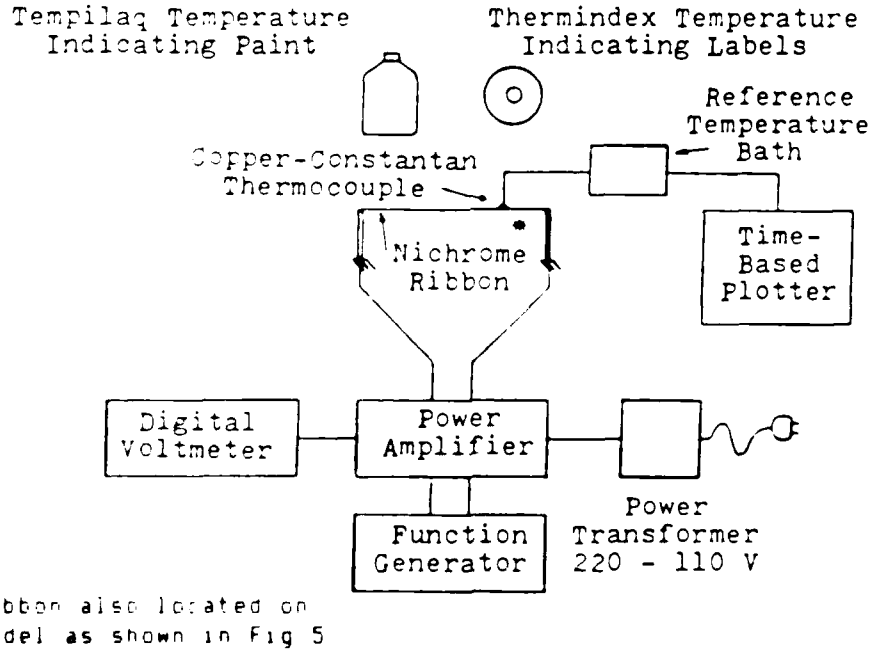

Fig 4. Equipment Arrangement for Ribbon Heating Experiments.

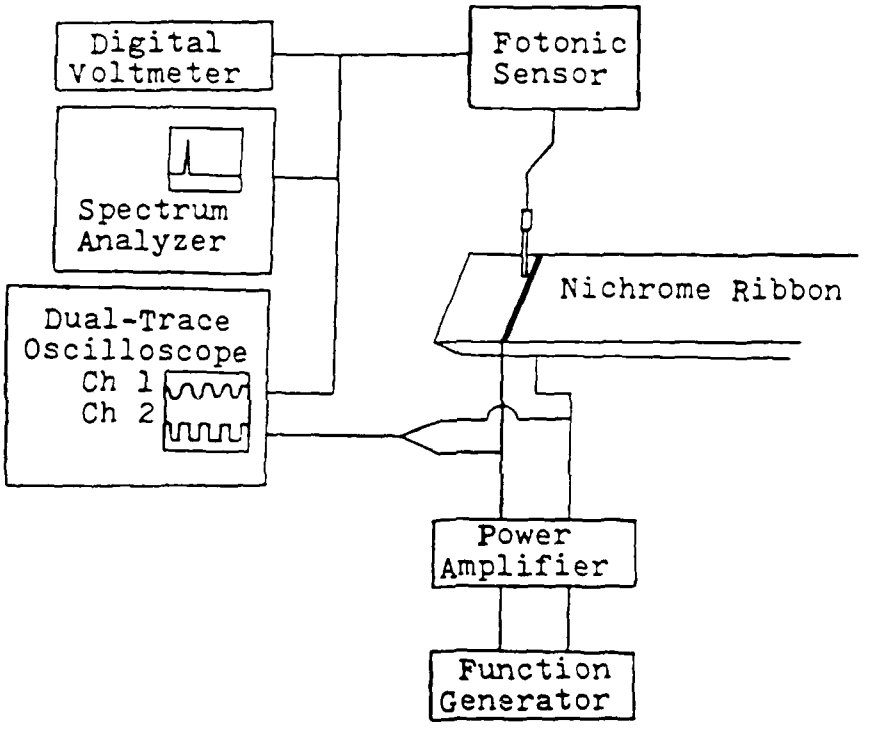

Fig 5. Equipment Arrangement for Ribbon Vibration Experiments.

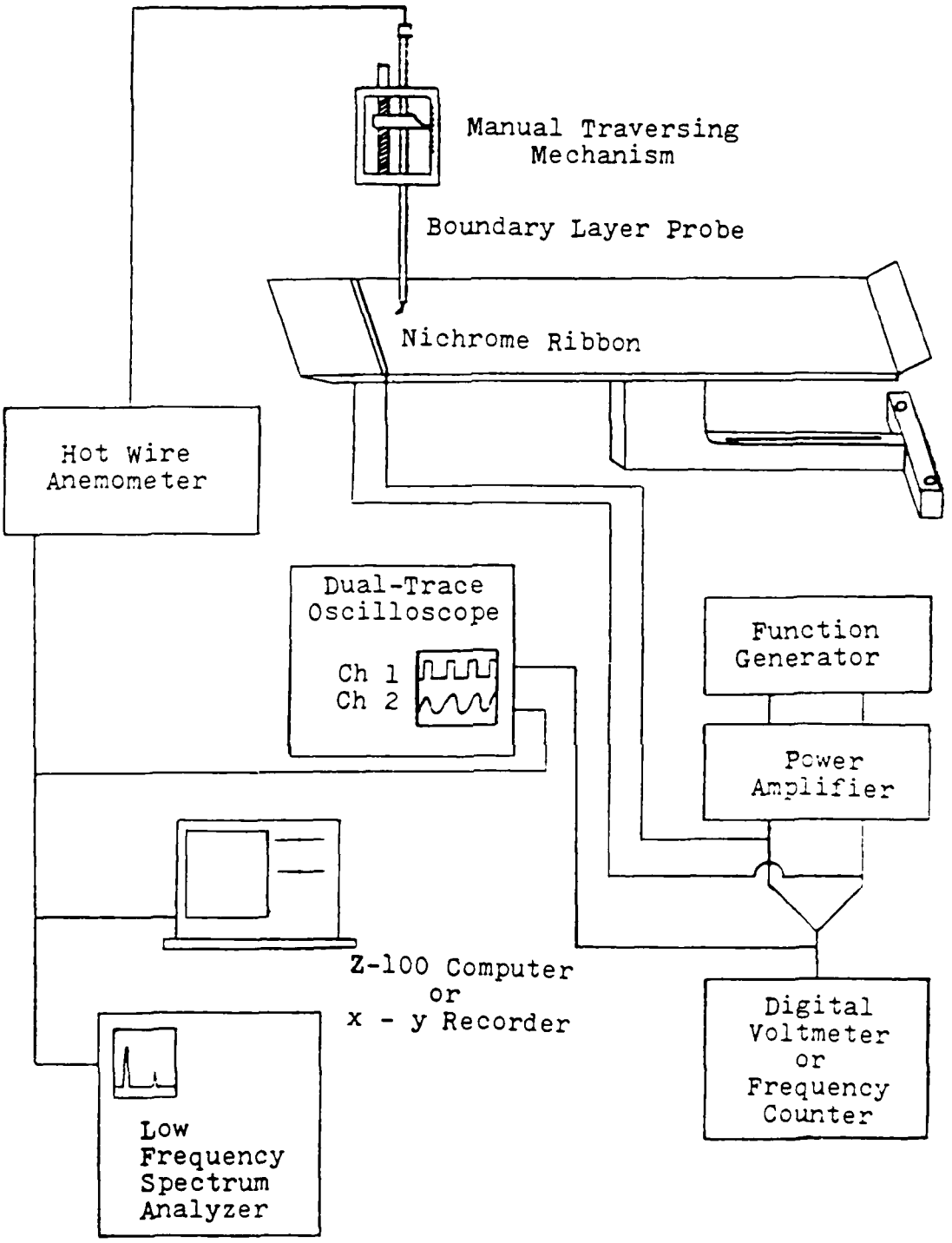

Fig 6. Equipment Arrangement for Boundary Layer Experiments.

The flat plate model configurations used in both wind tunnel facilities are shown in Fig 7. Models 1 through 3 were used in the AFIT wind tunnel, and Models 4 through 6 were used in the VKI wind tunnel. Model 1 is the Configuration 5 model used by Kudelka (11), with an additional groove located 127 mm from the leading edge. This model was too short to observe the development of the boundary layer disturbances downstream of the ribbon. To provide this capability, longer models were fabricated from 11-mm thick fiber reinforced phenolic. Model 2 is 0.76-m long and 0.20-m wide. Because the model did not completely span the 0.23-m wide test section, flow blockage due to the large support beneath the model caused large variations in the pressure gradient over the surface. This influence is illustrated in Fig 35 of Appendix A. Model 3 shows the addition of two side panels to Model 2. This model now completely spans the wind tunnel test section and supports the development of a nearly "flat plate" boundary layer. The boundary layer velocity profiles, at three streamwise locations along this model, closely resemble the flat plate boundary layer profiles given by the Blasius solution. These profiles are shown is Figs 36 through 38 of Appendix A. Model 4 is the same basic plate as Model 3 with wider side panels to accomodate the 0.28-m wide test section of the VKI facility. Model 5 is 0.15-m longer than Model 4 and was designed to provide additional laminar boundary layer information between 0.7 and 0.9 m from the leading

edge. However, the benefits of this model were not realized because the wind tunnel turbulence level (0.5 percent) made it difficult to maintain laminar flow over the rear 0.2 m of this model. The leading edge of Model 4 was reshaped to form a 2-to-1 half ellipse. This model, Model 6, was designed to minimize the leading edge flow disturbance by providing a smoother path for the streamlines in the immediate vicinity of the leading edge. All six models were equipped with a flap to adjust the oncoming streamlines with respect to the model leading edge. Deflecting the flap upward was equivalent to putting the plate at a negative angle of attack. This enhanced the boundary layer stability by creating a slightly favorable pressure gradient near the leading edge and by eliminating the formation of a stagnation bubble on the upper surface of the model. The fixed flap of Model 1 was 0.15-m long and deflected 30 deg. Models 2 through 6 had 0.07-m long flaps which were adjustable from 0 to 50 deg.

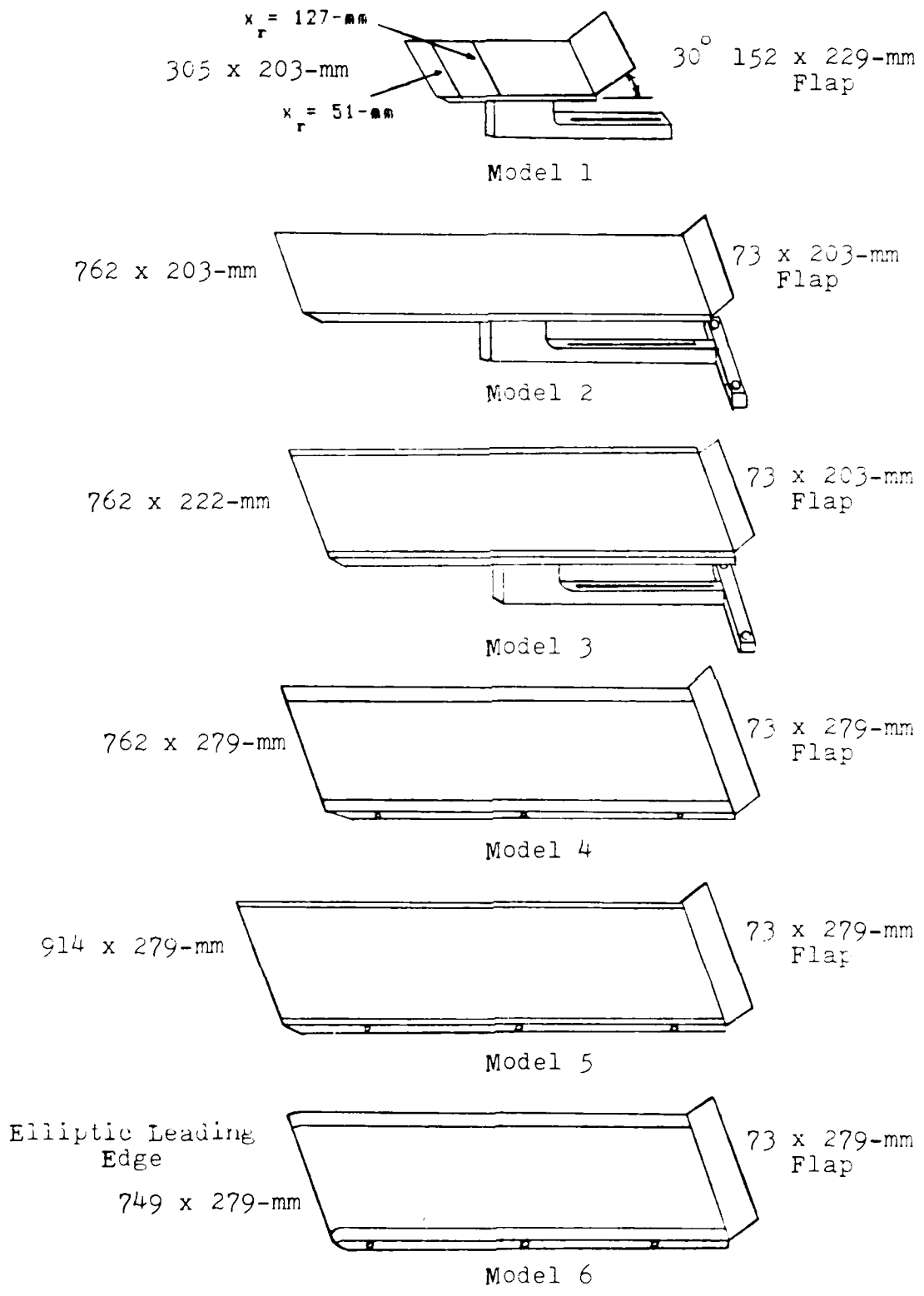

Fig 7. Flat Plate Model Configurations.

The dimensions and resistances of the Nichrome ribbons used throughout the experiments are given in Table II. The ribbons were placed on or near the surface of the model, perpendicular to the flow direction. Three methods were used to mount the ribbons to the models. The first was to rest the ribbon on the model surface and wrap the ends around the edges of the model (Fig 8a). Spring tension was then applied from a location beneath the model in order to take up slack in the ribbon as it expanded during heating. With this design, the ribbon could be located at any streamwise position along the model surface. The second method was to fix the ribbon to the surface with glue. This method was used to determine the influence of ribbon heating alone, no vibration, on the boundary layer stability. The fixed ribbon locations used in the experiments were 89 and 254 mm from the model leading edge. The third method is shown in Fig 8b. This device was only used with Model 6. The streamwise placement of the ribbon was fixed at 127 mm from the leading edge, however, the distance off the plate, y_r, could be varied. Tension was applied in-line with the ribbon using a spring attached to one end. This force was monitored with a strain gage balance attached to the other end of the ribbon.

Table II. Dimensions and Resistances of Nichrome Ribbons

Ribbon	1*	2	3	4	5	6	7	8
Dimensions (mm)	0.71 x 0.061 x 225	1.2 x 0.127 x 254	0.79 x 0.127 x 222	0.79 x 0.127 x 254	1.59 x 0.127 x 305	0.79 x 0.127 x 305	1.59 x 0.127 x 267	1.59 x 0.127 x 209
Resistances (ohms)	4.84	2.18	3.35	3.77	2.11	4.38	1.75	1.20

* Same ribbon as that used by Kudelka (11).

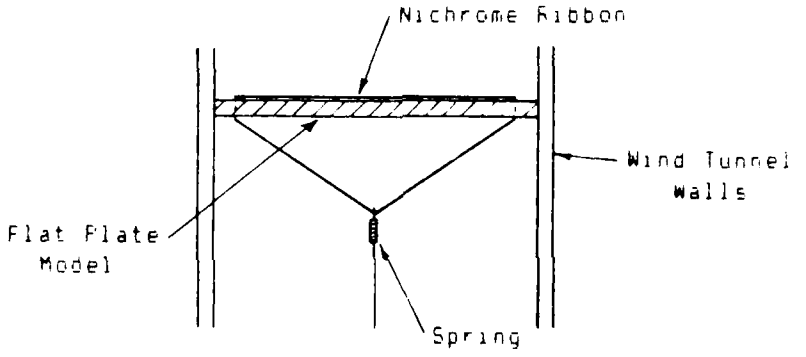

a. Method 1

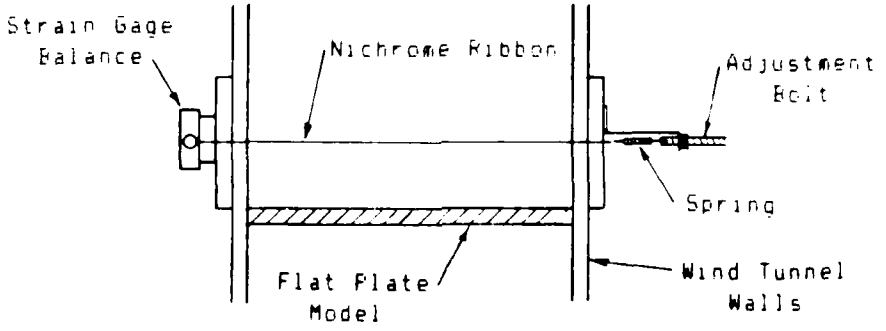

b. Method 3

Fig 8. Ribbon Tension Systems.

IV Experimental Procedure

The experiments were structured to provide fundemental information on the physical response of the ribbon to a given input, and the subsequent response of the boundary layer to the presence of the ribbon.

The Nichrome ribbon was placed transversely on a flat plate model in a shallow groove (Model 1), directly on the surface, or a distance y_r above the surface. Spring tension, glue, or a special ribbon traversing device was used to keep the ribbon near the model surface (Fig 8). The ribbon was excited using a function generator and amplifier. The function generator produced an asymmetric square wave having an on-off ratio of 1 to 7. This signal was amplified to provide the desired voltage across the ribbon. The resulting input was monitored using an oscilloscope and digital voltmeter or frequency counter.

Ribbon Characteristics

The physical response of the Nichrome ribbon to a pulsed voltage input was examined in terms of: 1) the heating characteristics, 2) the ribbon time constant, and 3) the frequency and amplitude of the resulting ribbon vibration.

The heating characteristics of the Nichrome ribbon were investigated using both a thermocouple welded to the ribbon surface and temperature indicating paints and labels (Fig

4). The thermocouples were spot welded to Ribbons 6 and 7. They were placed 83 mm from the end of Ribbon 6 and 127 mm from the end of Ribbon 7. The thermocouples were made of copper and constantan wires, 0.2 mm in diameter. The change in voltage across the thermocouple circuit corresponded to a temperature change given by 42±2 $\mu V/^{\circ}C$ (4:162). The voltage produced by the thermocouple was either observed using a digital voltmeter or recorded using a time based plotter. The similarity in thickness and conductivity between the Nichrome ribbon and thermocouple wires creates the situation illustrated in Fig 9 (15:58-59). The heat produced by the ribbon is conducted toward the thermocouple wires and convected away, establishing a region of linearly decreasing temperature around the ribbon - thermocouple junction. The thermocouple indications can be corrected to reflect the actual temperature by specifying the proper correction factor. This was accomplished by using temperature indicating paints and labels in conjunction with the thermocouples. The Tempilaq indicating paints, for temperatures: 38, 52, 69, and 128°C, are characterized in terms of these certified melting temperatures. The Thermindex labels, for temperatures: 66, 166, 182, and 204°C, have a small grey dot in the center which instantaneously changes to black when the specified temperature is reached. Both the paints and labels were applied directly to the surface of the ribbon. For a fixed input frequency, the change in ribbon temperature with input

voltage was monitored using a variety of paints and labels. These experiments were performed for both a ribbon in free air and a model mounted ribbon exposed to different free stream velocities.

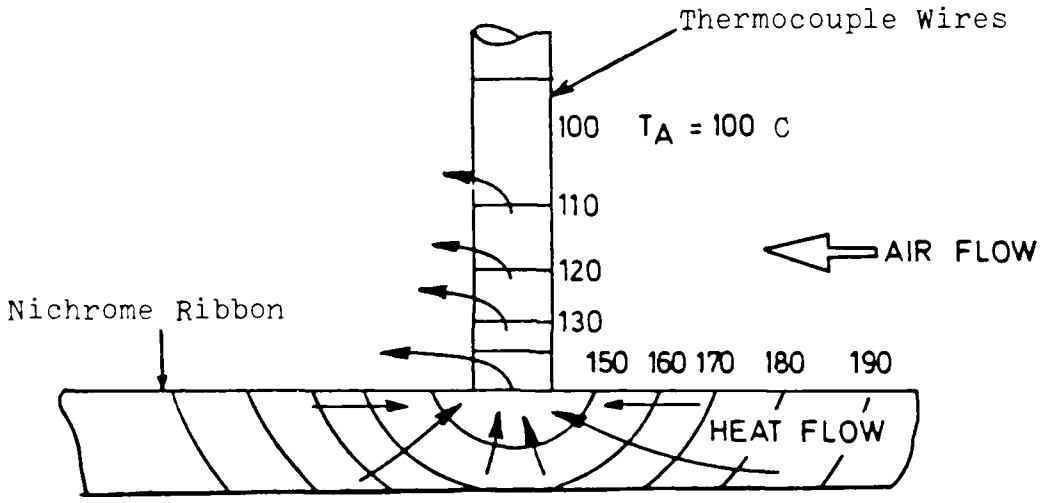

Fig 9. Temperature Variation in Ribbon due to Thermocouple.

The time response, or time constant, of the Nichrome ribbon was also investigated using a surface mounted thermocouple. The rate of heating was monitored by instantaneously applying a predetermined voltage and frequency to the ribbon, then recording the thermocouple output, or temperature rise, on the time based plotter. The cooling

rate was monitored in the same manner by instantaneously removing the input.

The frequency and amplitude of the ribbon vibration were measured using a KD-320 Fotonic sensor (Fig 5). The sensor was placed perpendicular to the ribbon with a sensor-to-surface gap of approximately 0.06 mm. The voltage output of the sensor reflected any change in the position of the ribbon. By channeling this output to an oscilloscope and spectrum analyzer, the frequency and amplitude of the ribbon response could be recorded. Photographs of the oscilloscope and spectrum analyzer traces were taken to make a permanent record of the response. This experiment was performed using Models 1 and 3; Ribbons 1, 2, and 3; and various free stream flow velocities.

Boundary Layer Response

The response of the boundary layer to the presence of a Nichrome ribbon placed on or near the surface of a flat plate model was examined using the apparatus shown in Fig 6. The position of the hot wire anemometer in the boundary layer was selected based on the location of the largest disturbances. The maximum amplitude of the TS type disturbances lies at a constant non-dimensionalized distance from the surface of the model (22:479). This distance is about 0.36. Throughout the experiments, the boundary layer probe was positioned to provide maximum amplitude readings. The general trends for the anemometer position in the

y-direction were to increase y_a with increasing x. The traversing capability of the anemometer probe depended on the wind tunnel being used. The VKI facility allowed the probe to move continuously in all three directions. The AFIT facility provided continuous movement in the y-direction, discrete movement in the streamline direction, and no movement along the span of the model. In both facilities, the boundary layer development was followed by moving the probe to different streamwise locations.

Before the ribbon was placed on the surface of a model, the boundary layer probe was used to obtain velocity and turbulence profiles of the boundary layer along the length of the model. This information was used to estimate flap angles and flow velocities at which the boundary layer remained laminar over the entire length. This also indicated the uniformity of the pressure gradient over the surface of the model.

The influence of the ribbon on the boundary layer was considered for three cases: 1) the ribbon held close to the surface using spring tension, 2) the ribbon fixed to the surface with glue, and 3) the ribbon placed a distance y_r above the surface of the model using a ribbon traversing mechanism.

The boundary layer probe was initially positioned slightly downstream of the ribbon. As the ribbon responded to the various input voltages and frequencies, the boundary probe would detect the resulting disturbance in the boundary

layer. The response was seen by channeling the hot wire anemometer output to either an oscilloscope or spectrum analyzer. The evolution of these propagating boundary layer disturbances was obtained by photographing the oscilloscope and/or spectrum analyzer traces as the probe moved in discrete steps downstream of the ribbon.

The influence of the ribbon along the span of the model was investigated using Model 4. The boundary layer probe was placed 25 mm behind the ribbon. Turbulence profiles at different locations along the span, ± 50 mm from the centerline, were obtained by plotting the output of the anemometer and displacement potentiometer (records y position of the probe) using the x-y recorder.

V. Results and Discussion

Ribbon Heating and Time Constant Results and Discussion

The thermocouple was the primary device used to determine the heating and time constant characteristics of the Nichrome ribbon. However, the condition illustrated in Fig 9 suggests the need for a correction to the thermocouple temperature indication. This was accomplished using a variety of temperature indicating paints and labels in conjunction with the thermocouple. The ribbons in these experiments were free standing and not subjected to forced airflow. Figure 10 and Table III show the comparison between the thermocouple temperature indications and the paint/label results for Ribbons 6 and 7. A least squares fit to both sets of data gives the relationship between the thermocouple prediction and the actual ribbon temperature. This relationship is indicated by the slopes of the two lines. For Ribbon 6, the slope $\Delta T_{tc}/\Delta T_{p}$ is 0.61, and for Ribbon 7, the slope is 0.62. Expanding these correction factors to thermocouple results obtained under forced flow conditions, an accurate estimate can be made of the actual ribbon temperature. The ribbon time constant can also be obtained directly from the thermocouple data because of the linear relationship between the thermocouple indication and actual ribbon temperature.

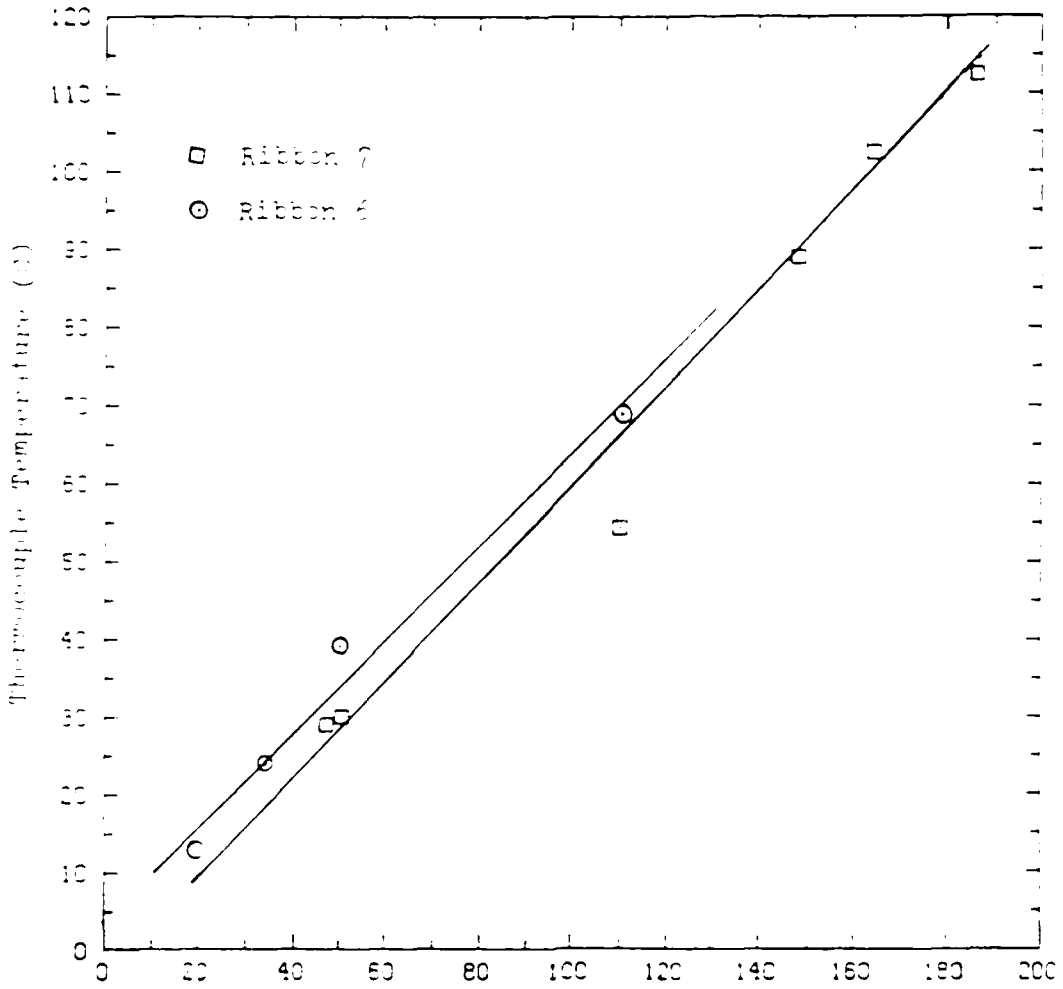

Fig 10. Comparison Between the Thermocouple Temperature Indication and Paint/Label Indication.

Table III. Thermocouple—Paint/Label Results

Ribbon	Input Voltage to Ribbon Vrms	Thermocouple Indication ΔT_{tc} °C	Paint/Label Indication ΔT_p °C
6	1.64	13	20[1]
	2.38	24	34[1]
	3.06	39	51[1]
	3.98	69	110[1]
7	1.75	29	48[2]
	1.84	30	51[1]
	2.56	55	110[1]
	3.48	89	148[2]
	3.66	103	164[2]
	3.81	113	186[2]

1 Paint Indication
2 Label Indication

The temperature of the Nichrome ribbon, in response to a voltage input, was determined using a thermocouple and the applicable correction factor. The variation in temperature with free stream velocity was investigated for Ribbons 6 and 7 mounted on the surface of Model 5. For Ribbon 6, the influence of input frequency and location on the model, x_r, were also investigated. Table IV presents the ribbon temperature results in terms of the change in temperature given by the thermocouple, ΔT_{tc}, and the corrected temperature change, ΔT_{corr}, for specific input conditions, free stream velocities, and ribbon locations.

Table IV. Results of Ribbon Heating Experiments.
y_r = 0.25 mm; T_{amb} = 18 °C; T_f = 38 °C;
k_f = 0.0268 W/mK; ν_f = 1.74x10^{-6} m^2/s

Row	Ribbon Voltage (Vrms) Dimensions (mm) Resistance (Ω)	x_r mm	Freq Hz	U_∞ m/s	η *	u_r m/s	Re_{lf} $u_r l/\nu$
1	7	127	109	0.0	—	—	—
2	4.9			5.7	0.409	0.8	72.9
3	1.59x0.127x276			7.0	0.452	1.0	94.5
4	1.75			8.1	0.487	1.9	119.6
5	6	229	104	0.0	—	—	—
6				5.8	0.907	0.6	26.4
7				7.1	0.999	0.8	36.1
8				8.2	0.964	1.0	44.5
9	6.24	114		0.0	—	—	—
10				5.8	0.493	0.8	37.5
11				7.1	0.479	1.1	51.4
12	0.79x0.127x905			8.2	0.515	1.4	64.0
13				9.1	0.545	1.6	75.1
14	4.98		80	9.1	0.545	1.6	75.1
15			91				
16			100				
17			913				

Row	Column 1 ΔT_{tc} °C	2 ΔT_{corr} °C	3 h^{**} W/m^{2}K	4 τ sec	5 τ_{exp} sec
1	219.0	959.2	—	—	7.50
2	29.0	46.8	85.2	2.55	1.95
3	24.6	39.7	97.0	2.24	1.80
4	21.7	35.0	109.6	1.98	1.75
5	102.4	167.9	—	—	No Data
6	40.0	65.6	102.8	1.97	
7	35.7	58.5	120.4	1.68	
8	33.3	54.6	139.3	1.52	
9	100.5	164.8	—	—	5.75
10	37.8	62.0	122.7	1.65	1.70
11	34.4	56.4	149.7	1.41	1.50
12	31.3	51.3	160.1	1.26	1.40
13	29.5	48.4	179.8	1.16	1.30
14	29.3	49.0	179.8	1.16	1.30
15	29.3	49.0			1.30
16	29.4	48.2			1.30
17	29.8	48.9			1.30

* $\eta = y_r (U_\infty / x_r \nu_f)^{1/2}$ determines u_r / U_∞.

** Based on eq (8)

The temperature variation of the Nichrome ribbon over an input cycle is illustrated in Fig 11.

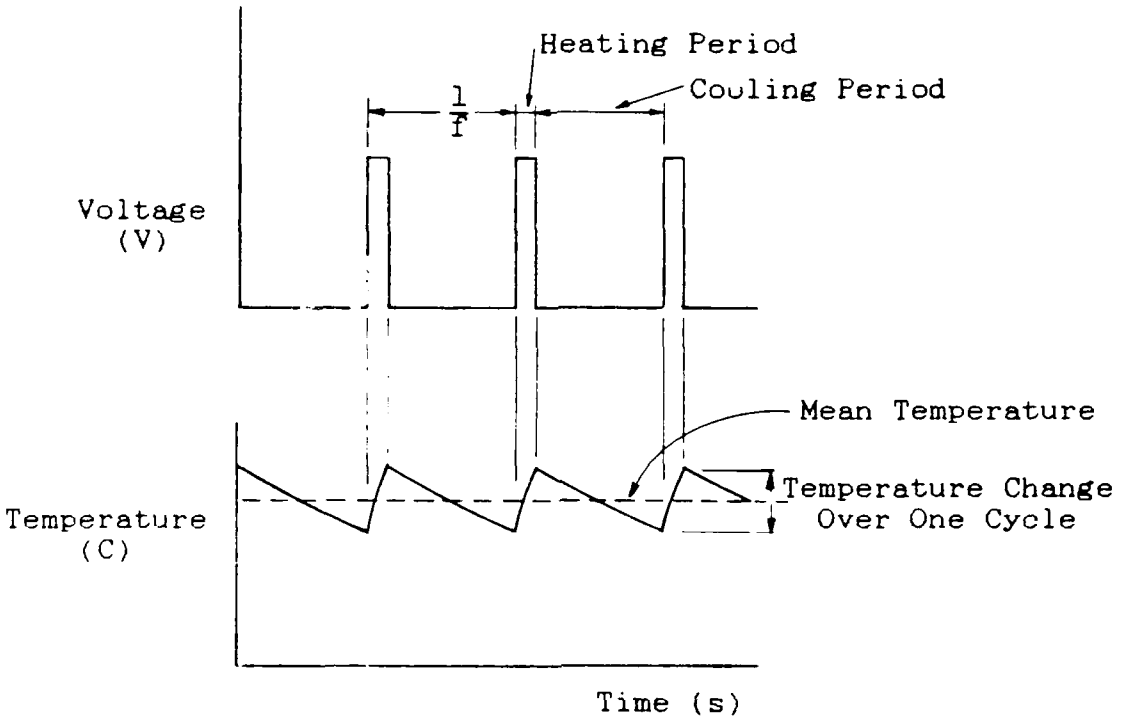

Fig 11. Temperature Variation of the Nichrome Ribbon Over an Input Cycle.

This variation in temperature is determined by the response time, or time constant τ, of the Nichrome ribbon. Using the properties of Nichrome I in Table I, the time constants for Ribbons 6 and 7, written in terms of the convective heat transfer coefficient h, are:

$$\tau_6 = 202/h$$

and $$\tau_7 = 217/h,$$

where h is in units of W/m^2K and τ is in seconds. The

value for h was calculated using eq (10).

The ribbon time constant was also experimentally determined using the thermocouple arrangement. A typical thermocouple voltage trace, converted to a temperature change, is given in Fig 12. The time required for the ribbon to reach its mean temperature depended upon the flow conditions. The time was about 30 s for a forced flow condition, but increased to 150 s for a no flow condition. After the mean temperature was reached, the input was instantaneously removed. This corresponds to the point of rapidly decreasing temperature in Fig 12. The time constant represents the time it takes the ribbon to go from:

$$T = \Delta T_{max} + T_{amb}$$

to:

$$T = 0.368\ \Delta T_{max} + T_{amb}.$$

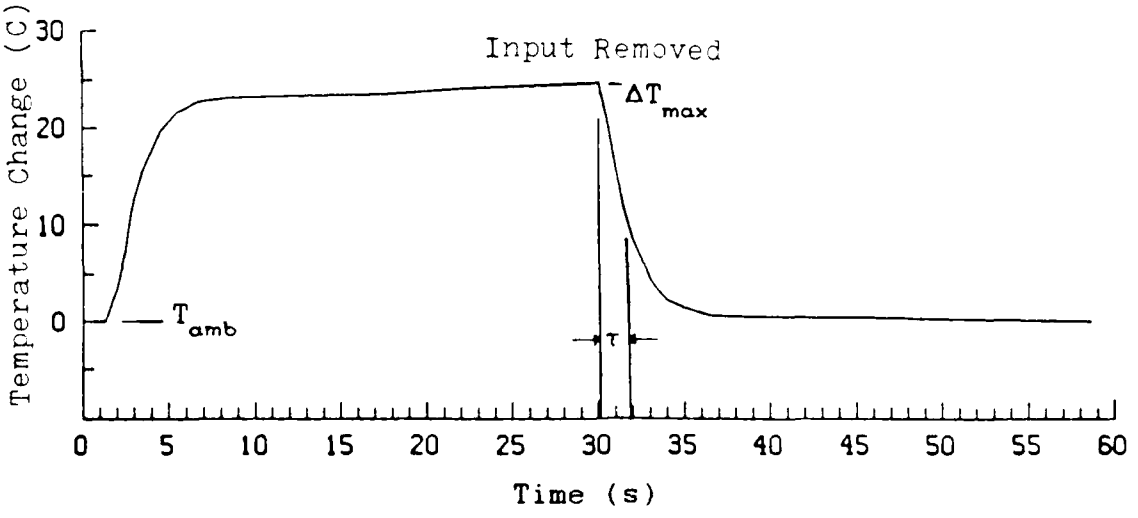

Fig 12. Thermocouple Measurement for the Change in Ribbon Temperature with Time After Instantaneously Removing the Ribbon Input.

The values of the calculated time constants τ, based on the convective heat transfer coefficient of column 3 (Table IV), and the experimentally obtained values τ_{exp} are presented in columns 4 and 5 of Table IV. The order of the time constant for the experimental and calculated values are in excellent agreement.

The temperature variation over a single input cycle, shown in Fig 11, can be estimated using eq (8) and representative values found in row 10 of Table IV. Equation (8) is applied separately to the heating portion, where q_v is approximately $8V_{rms}^2/R$; and the cooling portion, where $q_v = 0$. For heating over the first one-eighth of the cycle, eq (8) becomes:

$$\frac{T_{max} - T_o}{18 - T_o + 8V_{rms}^2/RAh} = 1 - \exp\left(\frac{-1}{8f\tau_{exp}}\right),$$

or:
$$T_{max} = 0.7433 + 0.99929\ T_o.$$

For cooling over the remaining seven-eighths, eq (8) becomes:

$$\frac{T_{min} - T_o}{18 - T_o} = 1 - \exp\left(\frac{-7}{8f\tau_{exp}}\right),$$

or:
$$T_{min} = 0.08886 + 0.99506\ T_o.$$

Taking T_o to be 62.0 °C (row 10, column 2 values of Table IV), the temperature difference between the beginning and end of a complete cycle is approximately:

$$T_{max} - T_{min} = 0.92\ ^{\circ}C.$$

The small temperature change over the input cycle indicates that the ribbon reaches an almost constant temperature for a given voltage and heat loss rate to the surroundings. The change in ribbon length accompanying this small temperature change can be estimated by knowing the coefficient of thermal expansion for Nichrome. The coefficient of thermal expansion is 0.0000137 mm/mm$^{\circ}$C, as given by the manufacturer. After the initial expansion of the ribbon as it is heated to the mean value, changes in the overall ribbon length during a cycle are calculated using the coefficient of thermal expansion and the approximate temperature change over that cycle (Fig 11). For a ribbon 305-mm-long, the change in length corresponding to a temperature change of 0.92°C is only 0.0038 mm. This value is influenced by the input frequency. Lower input frequencies give more time for heating and cooling over a cycle, resulting in larger temperature and length changes.

Ribbon Vibration Results and Discussion

The vibration characterics of the Nichrome ribbon were investigated using the apparatus shown in Fig 5. The objective of these experiments was to relate the voltage and frequency input, free stream flow velocity, and tension applied to the ribbon to the resulting amplitude and

frequency of the ribbon vibration. The complex interaction among these parameters made quantitative correlations extremely difficult. The results presented here represent basic trends as each parameter was individually varied.

A typical ribbon vibration response to a pulsed voltage at 68 Hz is shown in Figs 13 and 14. The resulting vibration consists of many multiples of this input frequency. Figure 13 is an oscilloscope trace of the Fotonic sensor voltage output. The sensor output reflects any change in the ribbon position with time. The exact frequencies associated with the movement of the ribbon, or vibration, are seen by sending this same output through a low frequency spectrum analyzer. Figure 14 quantifies the vibration response in terms of component frequencies. The frequency peaks indicated by the spectrum analyzer output, with the signal amplitude in parentheses, correspond to 68 (52), 136 (10.4), 204 (7.3), 272 (96.1), 340 (4.88), 472 (10.7), 540 (3.66), and 744 Hz (2.14 mV).

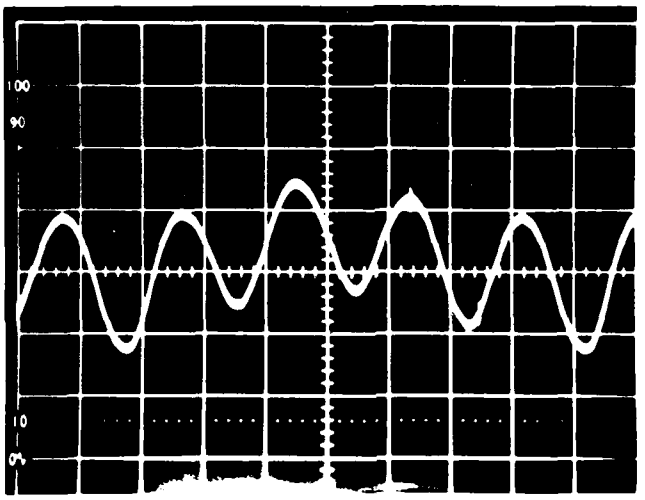

Fotonic Sensor Output (.2V/div)

Time (2ms/div)

Fig 13. Oscilloscope Trace of Typical Ribbon Vibration. Input to Ribbon 3: 68 Hz at 5.35 V_{rms}; Flow Velocity = 0 m/s; Model 3

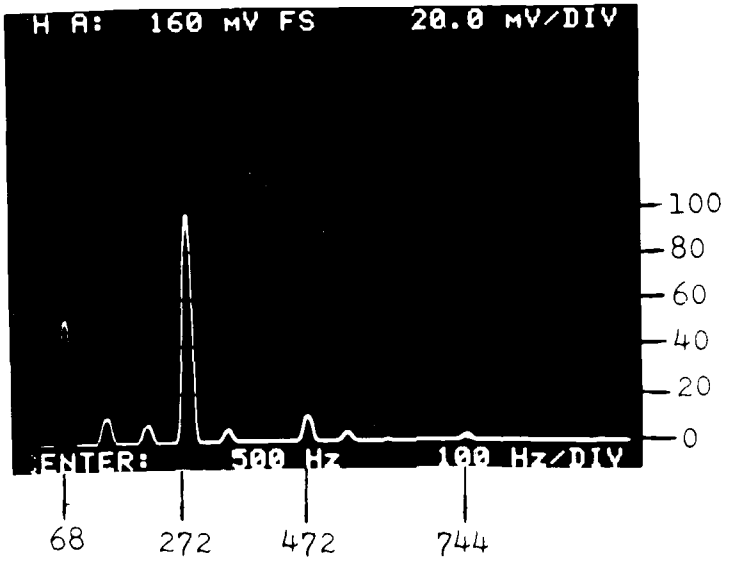

Fotonic Sensor Output (mV)

Frequency Hz

Fig 14. Spectrum Analyzer Trace of Typical Ribbon Vibration. Input to Ribbon 3: 68 Hz at 5.32V_{rms}; Flow Velocity = 0 m/s; Model 3

Changes in the input frequency, input voltage, ribbon tension, and/or free stream velocity resulted in changes to the ribbon vibration characteristics. The responses ranged from multi-frequency vibrations, similar to Fig 14, to a resonant vibration. The resonant response was a single frequency, large amplitude vibration. For fixed input voltage, tension, and free stream conditions, the resonant vibration could only be triggered by certain input frequencies. These frequencies had an integral multiple equal to the resonant frequency. The next three figures show how the frequency of the resonant response shifts with free stream velocity. Figures 15, 16, and 17 plot the amplitude of the vibration at or near the indicated resonant frequency. For example, Fig 15 indicates frequency inputs of 137, 208, and 417 Hz resulted in a ribbon vibration between 410 and 417 Hz. Input frequencies falling between those indicated for producing a resonant response resulted in greatly reduced vibration amplitudes at higher frequencies.

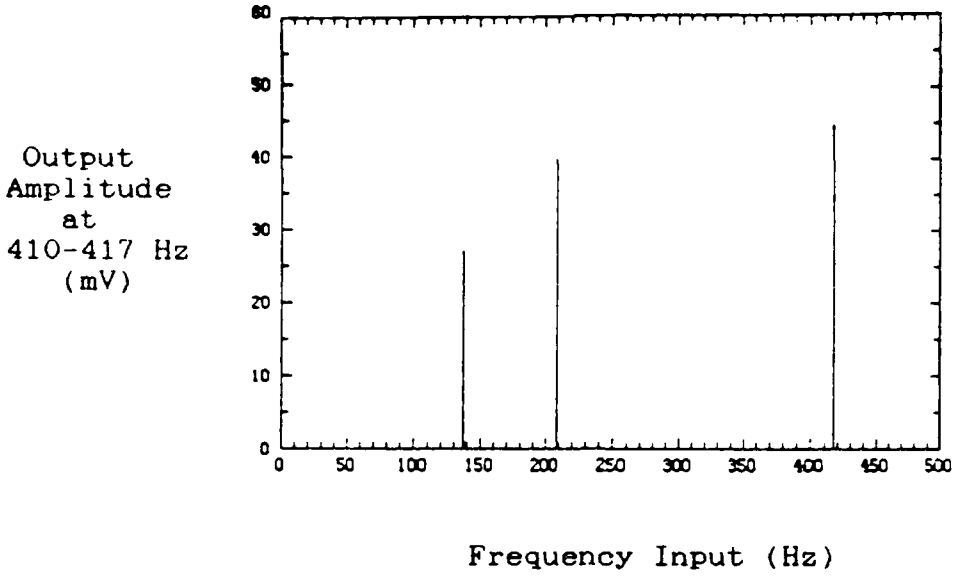

Fig 15. Ribbon Resonant Behavior - Free Stream Velocity 4.6 m/s. Fotonic Sensor Output; Ribbon 1

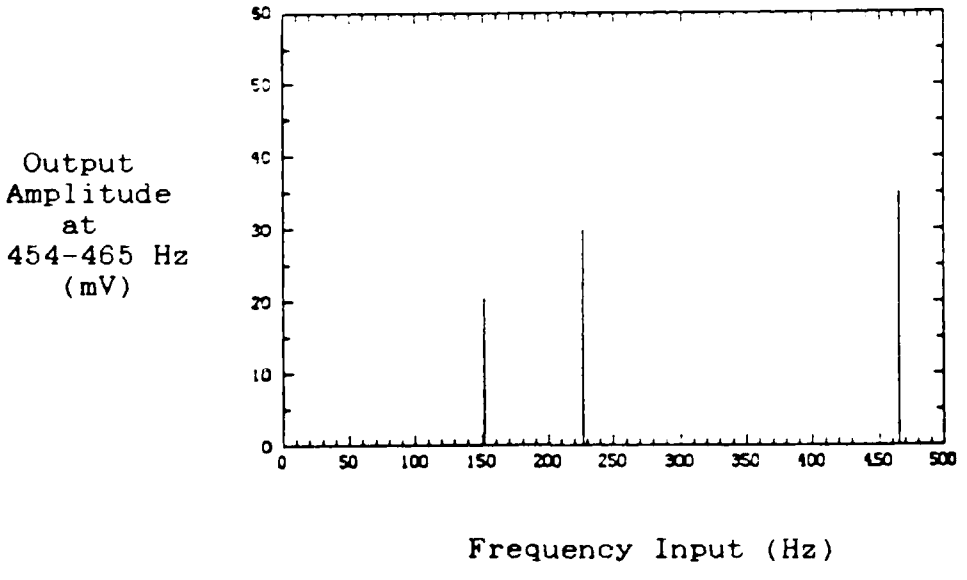

Fig 16. Ribbon Resonant Behavior - Free Stream Velocity 6.8 m/s. Fotonic Sensor Output; Ribbon 1

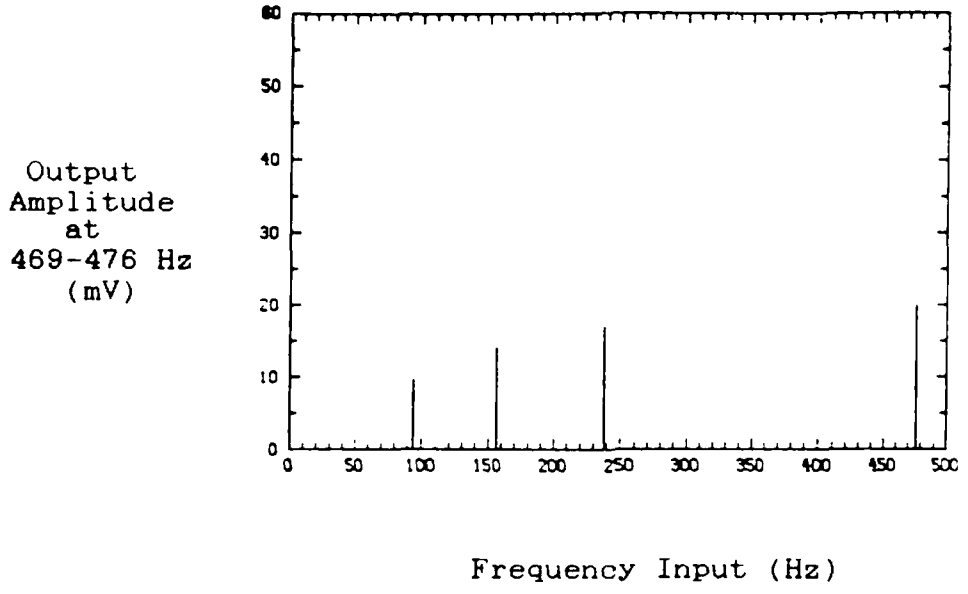

Fig 17. Ribbon Resonant Behavior - Free Stream Velocity 8.8 m/s. Fotonic Sensor Output; Ribbon 1

The effect of voltage and ribbon tension were similarily investigated. Increases in the input voltage to the ribbon reduced the frequency at which resonant conditions were noticed and increased the amplitude of the vibration. Increasing the ribbon tension had the opposite effect, increasing the frequency at which resonance occurred and decreasing the vibration amplitude. This ribbon vibration behavior is qualitatively supported by the theory discussed in Section II. The solution to eq (2) indicates that the fundamental, or first harmonic, of the natural frequencies is given by $\pi(\mathcal{T}/ml^2)^{1/2}$. Assuming the mass of the ribbon

remains constant, the fundamental frequency is proportional to the square root of the applied tension and inversely proportional to the length of the ribbon. The results of ribbon tension measurements, using the strain gage balance, indicate typical force values in the range of 0.5 to 1.0 N. For ribbon lengths of 0.3 m and areas of 0.1 mm^2 (Ribbon 6), the ribbon fundamental frequency falls in the range of 257 to 364 Hz. The fundamental frequency of the ribbon is largely dependent on the ribbon tension. Because spring force is proportional to the elongation of the spring, and the combined length of the ribbon and spring remains constant, the force applied to the ribbon must decrease as the ribbon elongates and increase as it contracts. Increasing the rate of convective cooling, by increasing the flow velocity over the ribbon, has just the opposite effect. According to the formula for calculating the ribbon natural frequencies, voltage increases will reduce the ribbon natural frequencies, and increases in tension will raise them.

Boundary Layer Results

The correspondance between the physical motion of the Nichrome ribbon and the boundary layer disturbances detected 25 mm downstream is shown in Fig 18. The Fotonic sensor output in Fig 18(a,b,c) represents the frequency composition of the ribbon vibration for three frequency inputs. The

movement of the ribbon can be compared to the boundary layer response shown in Fig 18(d,e,f). The anemometer sensed velocity disturbances having the identical frequencies as those detected by the Fotonic sensor. Figure 19 shows the location of several frequency components with respect to the Curve of Neutral Stability. For an anemometer location x_a = 0.127 mm and a free stream velocity of 7.3 m/s, the value for Re_{δ_1} is 430. All frequencies at this location lie in the stable region. As the boundary layer develops (Re_{δ_1} increases), only frequencies below 148 Hz will enter the instability region, all others will be naturally damped out by the boundary layer.

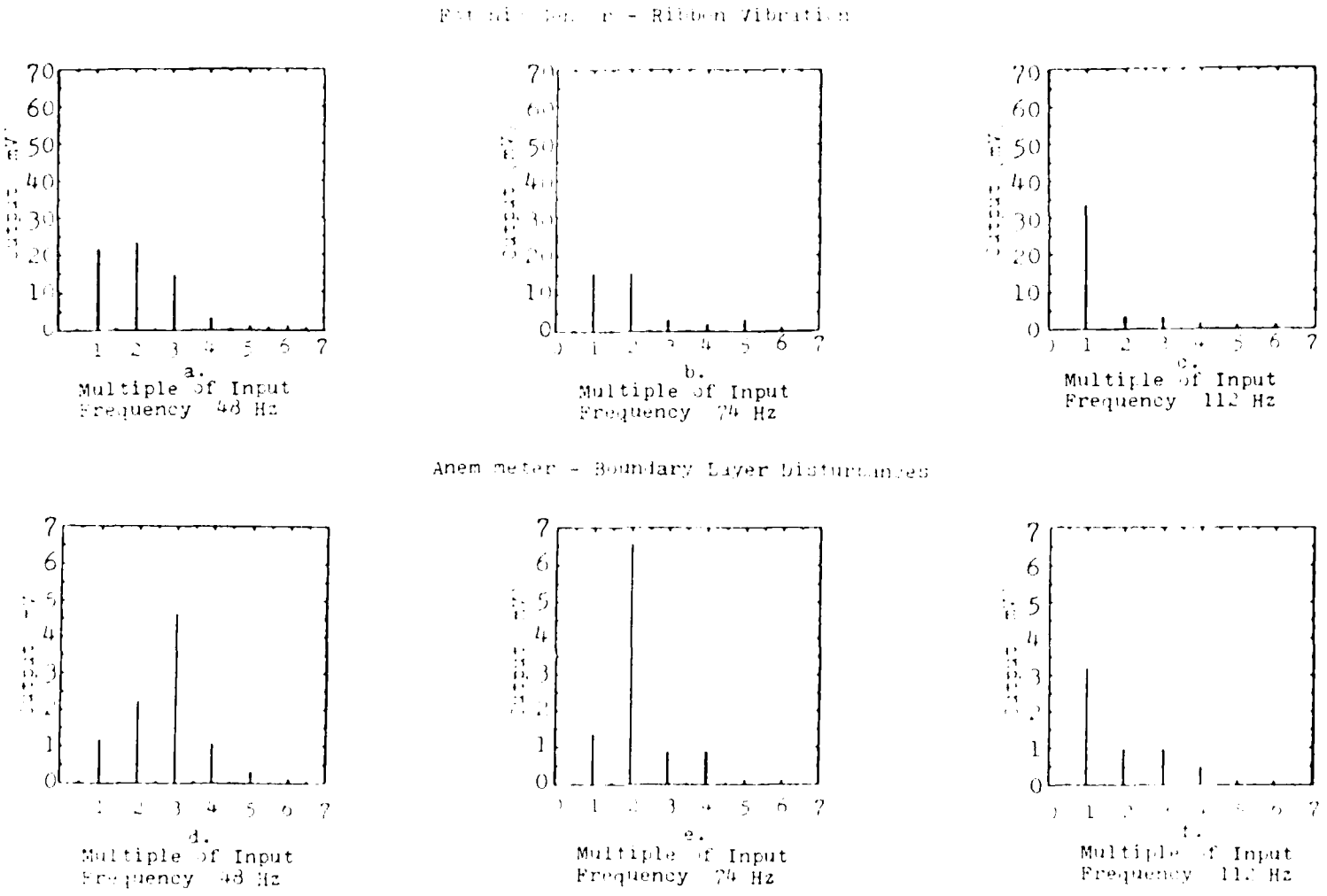

Fig 18. Correspondance Between the Ribbon Vibration and Boundary Disturbances. Free Stream Velocity: 7.2 m/s; Voltage Input: 5.3 Vrms; Ribbon 3; Model 3; x_r = 102 mm; x_a = 1.27 mm; y_a = .13 mm

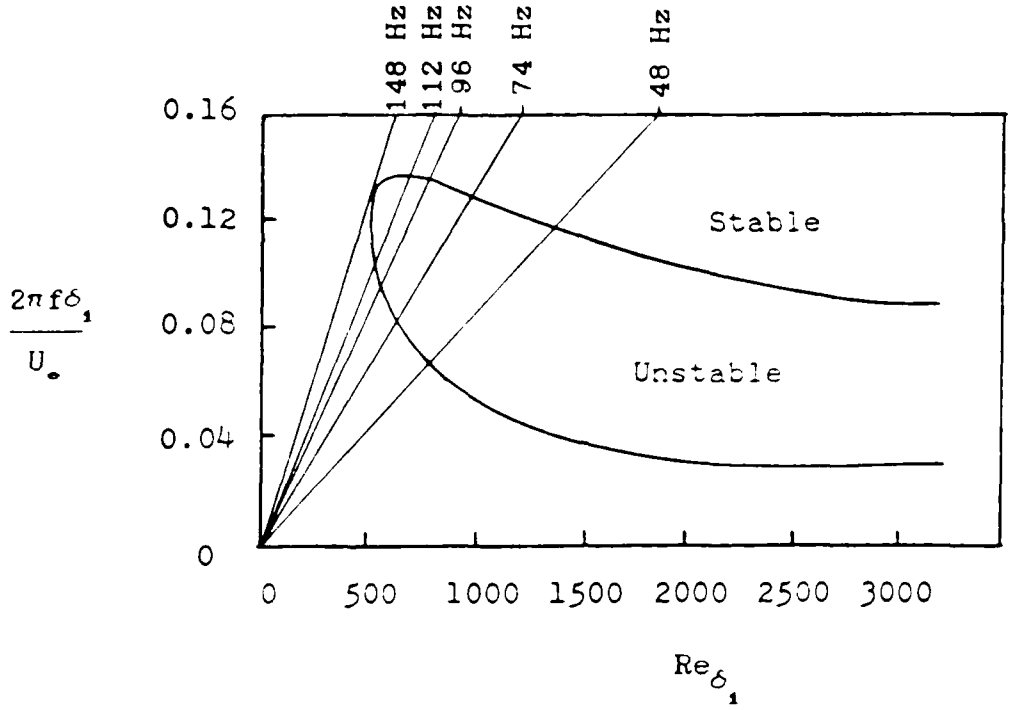

Fig 19. Curve of Neutral Stability for Figure 18.

The evolution of the ribbon induced boundary layer disturbances, in terms of frequency and amplitude, was seen by positioning the hot wire anemometer at different downstream locations. Figure 20 shows how the frequency composition changes as the boundary layer developed. In trace (a), the anemometer probe is located 25 mm downstream of the ribbon. The spectrum analyzer trace indicates the boundary layer has responded to the many frequency components of the ribbon vibration. Further downstream, higher frequency components rapidly disappear and the amplitude of low frequency components diminishes. Traces (e), (f), and (g) show how the boundary layer has suppressed all frequencies except the growing 87 Hz component.

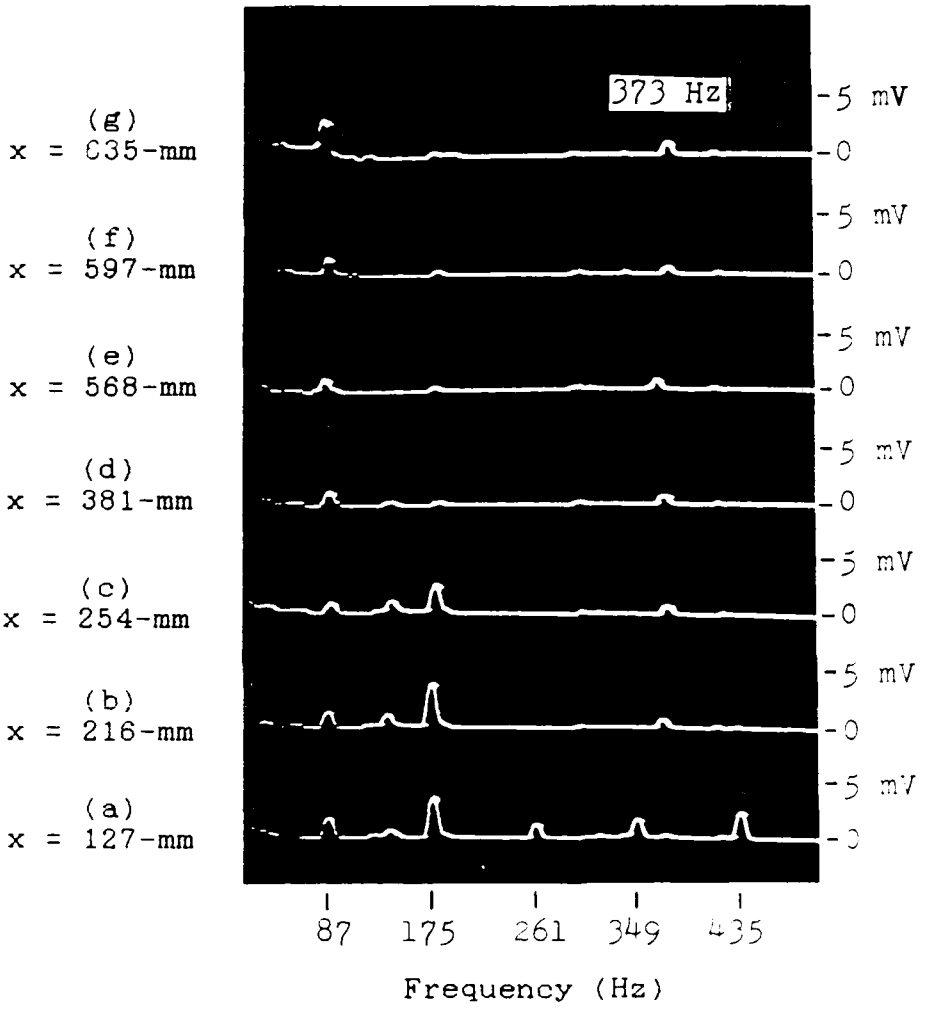

Fig 20. Spectrum Analyzer Traces at Seven Locations Downstream of the Vibrating Ribbon. Free Stream Velocity: 7.3 m/s. Model 3; Input to Ribbon 3: 87 Hz at 5.35 V_{rms}; Ribbon Location: x_r = 102 mm

The 373 to 379 Hz signal appearing in Fig 20 traces (b) through (g) do not originate from the vibrating ribbon. They are thought to be acoustic disturbances generated by the blade passage of the 6-bladed motor downstream of the test section. These signals were noticed after successfully reducing the wind tunnel vibration problems caused by the motor. These signals are related to the velocity of the flow through the wind tunnel test section. Figure 40 of Appendix A plots the motor vibration frequency versus test section velocity. For any test section flow velocity, the frequency of the acoustic disturbance can be determined by simply multiplying the motor vibration frequency by a factor of 6.

The apparent damping and amplification of the different frequency components in Fig 20 can be illustrated using the stability diagram in Fig 21. Constant frequency lines, or lines of constant $2\pi f\nu/U_e^2$, are shown for the 87, 175, 261, 348, and 435 Hz components. The position of these lines with respect to the instability region determines whether a certain frequency component will remain in the boundary layer. The only frequency passing through the instability region is at 87 Hz. According to Fig 21, the 87 Hz component of the propagating disturbance enters the instability region 0.2 m from the model leading edge (Re_{δ_1} = 600). And at 0.5 m (Re_{δ_1} = 875), the 87 Hz component approaches the point of maximum amplification.

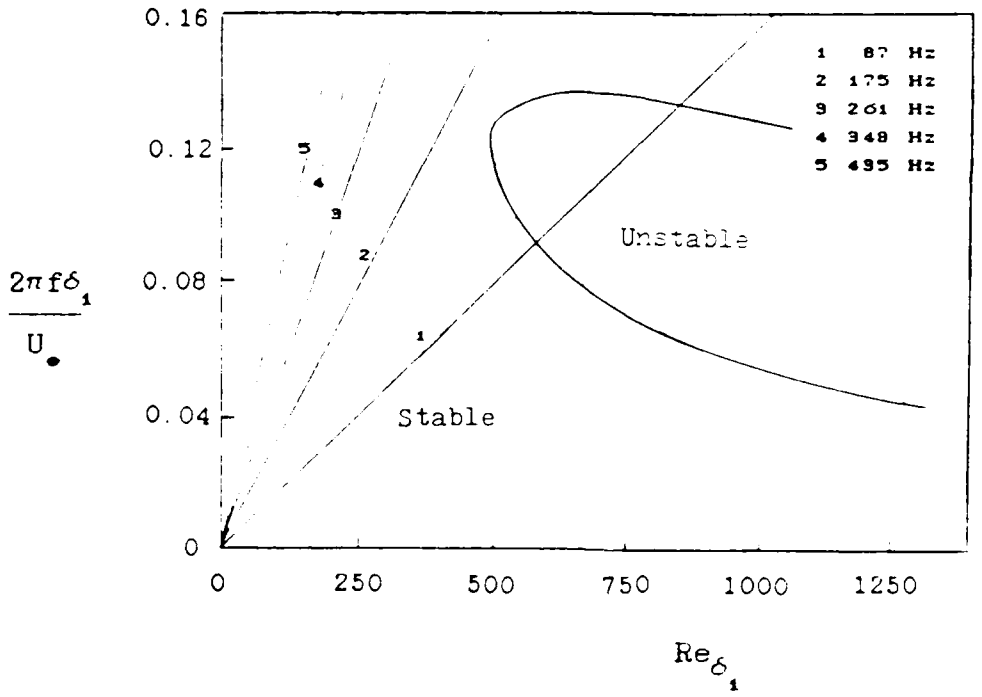

Fig 21. Curve of Neutral Stability for Figure 20. Disturbances.

Boundary layer experiments in the L-2A wind tunnel show a similar development in a series of hot wire anemometer traces. The oscilloscope traces in Fig 22 show the evolution of the disturbances excited by the Nichrome ribbon. The input frequency to the ribbon was 100 Hz. Immediately downstream of the ribbon, the boundary layer oscillations are dominated by a 300 Hz component (trace (a)). At a distance 166 mm from the ribbon, the 300 Hz frequency component has disappeared and the dominant frequency is 200 Hz (trace (b)). Trace (c) shows the presence of only the 100 Hz component 216 mm from the ribbon. The amplitude of this 100 Hz disturbance is much larger than either of the previous disturbances.

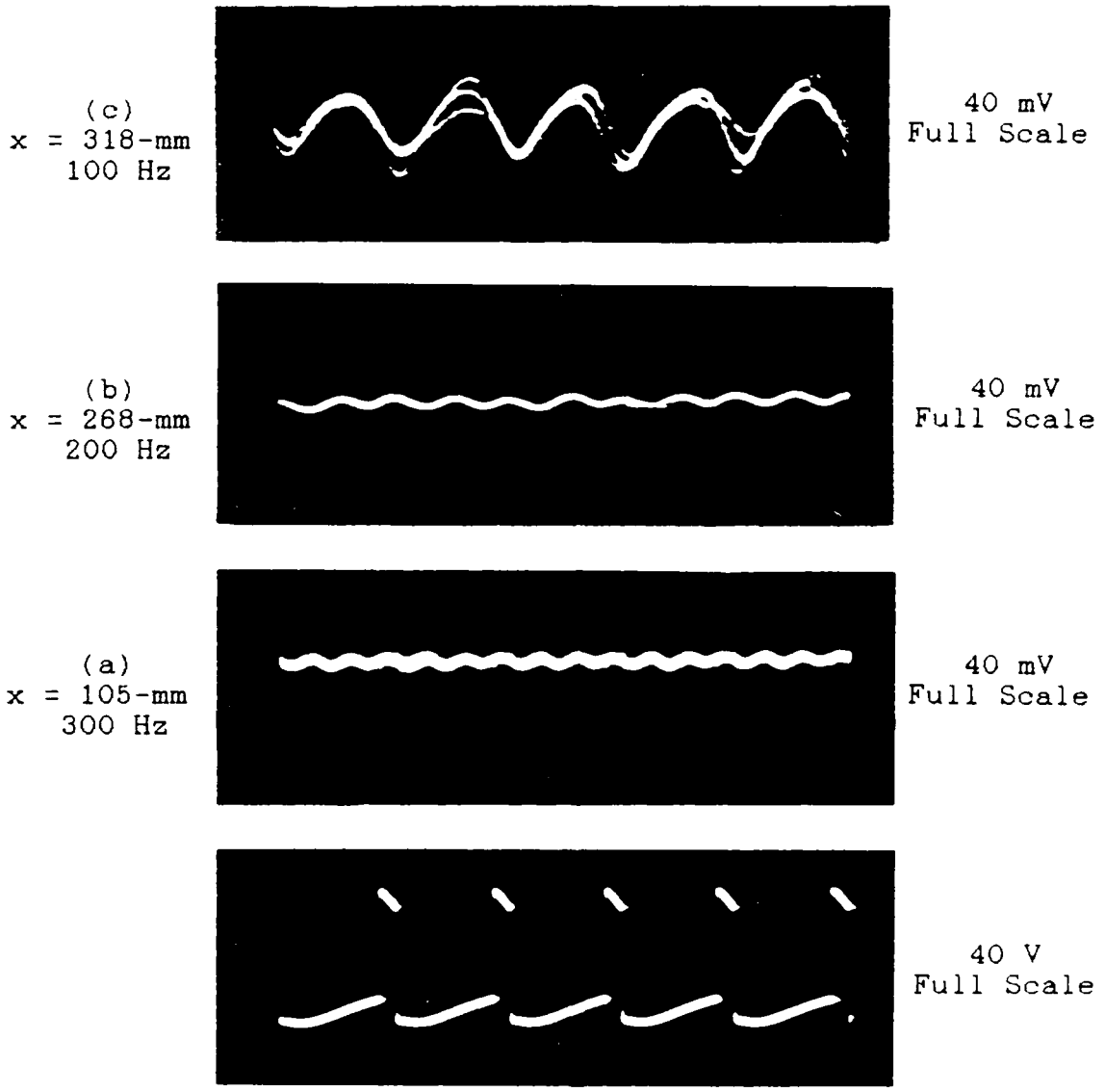

Input: 100 Hz
Ribbon Location: x_r = 102-mm

Fig 22. Oscilloscope Traces at Three Locations Downstream of a Vibrating Ribbon. Free Stream Velocity: 10 m/s; Model 4; Ribbon 6 Input: 100 Hz at 5.97 V_{rms}

The evolution of the propagating disturbances in Fig 22 is shown on the stability diagram in Fig 23. The three lines emitting from the origin represent the constant frequency lines for the 100, 200, and 300 Hz components. The 300 Hz line lies entirely in the stable region. This explains the complete damping of this component. The 200 Hz line passes through the instability region and reaches the point of maximum amplification near $Re_{\delta_1} = 730$ (Fig 23). Beyond this point, the 200 Hz disturbance is damped and the 100 Hz disturbance enters the instability region. This disturbance continued to be amplified until the pattern broke up and signs of turbulence appeared.

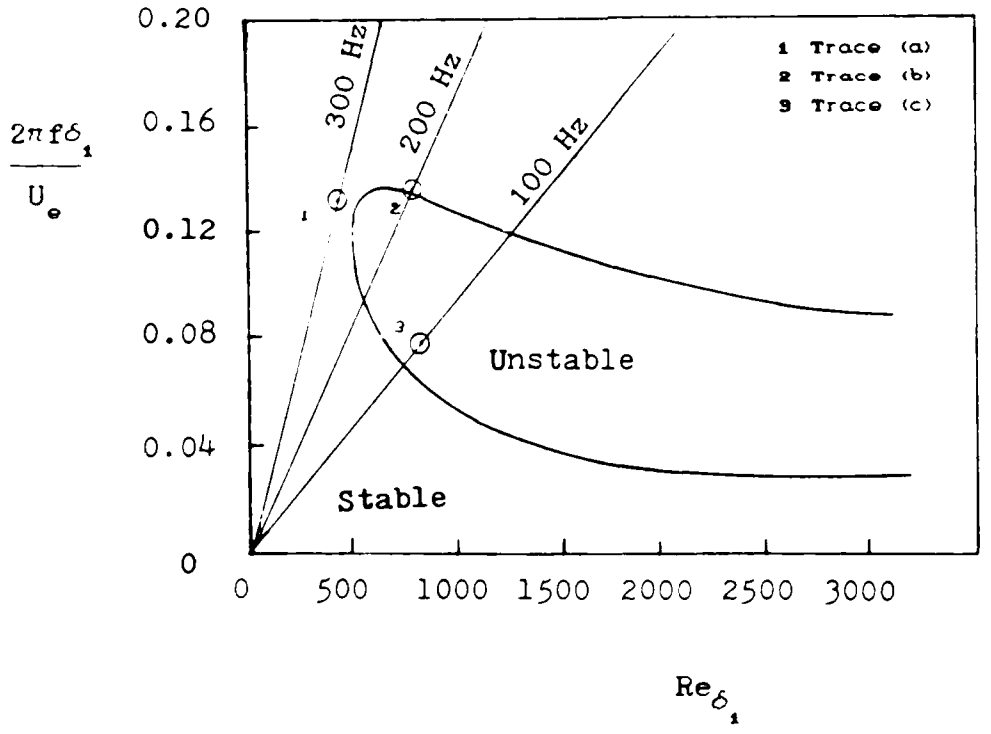

Fig 23. Curve of Neutral Stability for Figure 22 Disturbances.

Experiments to investigate the general amplification and damping of frequency components were performed by placing an anemometer probe 635 mm from the leading edge (533 mm downstream of the ribbon). At four different free stream velocities, the ribbon input frequency was varied from 30 to 216 Hz. The anemomter detected only specific ranges of frequencies at the downstream position. This range was influenced by the free stream velocity. Table V gives the free stream velocity and range of the observed frequencies at x = 635 mm. Two additional quantities are also calculated to aid in the comparison between the experimental results and two-dimensional stability theory. These quantities are the non-dimensional frequency, $2\pi f\delta_1/U_e$, and the Reynolds number based on the boundary layer displacement thickness, $U_e\delta_1/\nu$. Figure 24 shows the location of the observed frequency ranges with respect to the Curve of Neutral Stability.

Table V. Observed Frequency Ranges at x = 635 mm for Four Free Stream Velocities. Input Frequency Range to Ribbon 3: 30-216 Hz.

Edge Velocity (m/s) U_e	$Re_{\delta_1}^{*}$ $U_e\delta_1/\nu$	Observed Frequency Range Hz	Range of Parameter $2\pi f\delta_1/U_e$
7.5	973.8	60 - 96	.0967-.1547
8.5	1034.9	62 - 118	.0832-.1584
10.9	1173.9	70 - 156	.0644-.1435
12.6	1260.7	98 - 185	.0728-.1374

* $\nu = 14.9 \times 10^{-6}$ m^2/s; $\delta_1 = 1.7208x(Re_x)^{-1/2}$

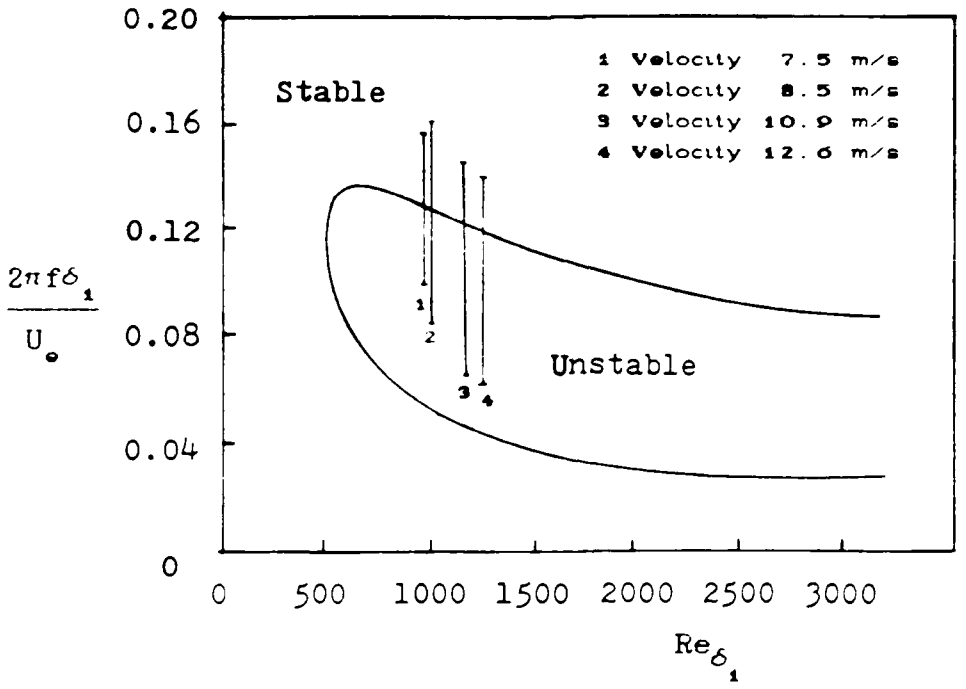

Fig 24. Curve of Neutral Stability for Table V.

The preceding results were obtained along the centerline of the models. The three-directional traverse at the VKI facility made it possible to observe the influence of the ribbon across the span. Figures 25, 26, and 27 show the anemometer response at different spanwise locations 25 mm behind a ribbon held to the surface by spring tension (Fig 8a). The disturbances, induced by the ribbon near the center of the plate (Fig 25), are sinusoidal with a frequency three times the input frequency. Away from the center of the model (Fig 26), the disturbances are not sinusoidal; instead, they exhibit random turbulent behavior. The input to the ribbon was then discontinued to see the effect of the non-vibrating ribbon. The turbulent behavior was still evident (Fig 27).

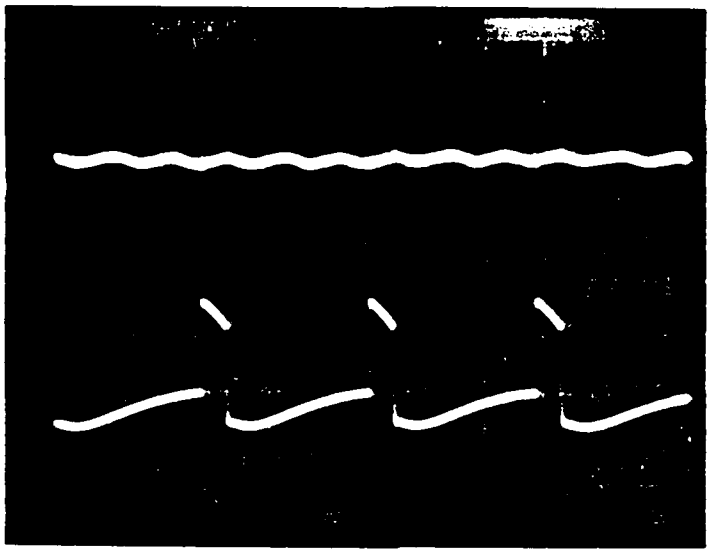

Fig 25. Spanwise Influence of Ribbon at z = -10 mm. Free Stream Velocity: 8.2 m/s; Model 4; Input to Ribbon 6: 71.4 Hz at 6.14 V_{rms}; x_r = 25 mm; $y_r \approx 0$ mm; x_a = 51 mm; y_a = 0.6 mm

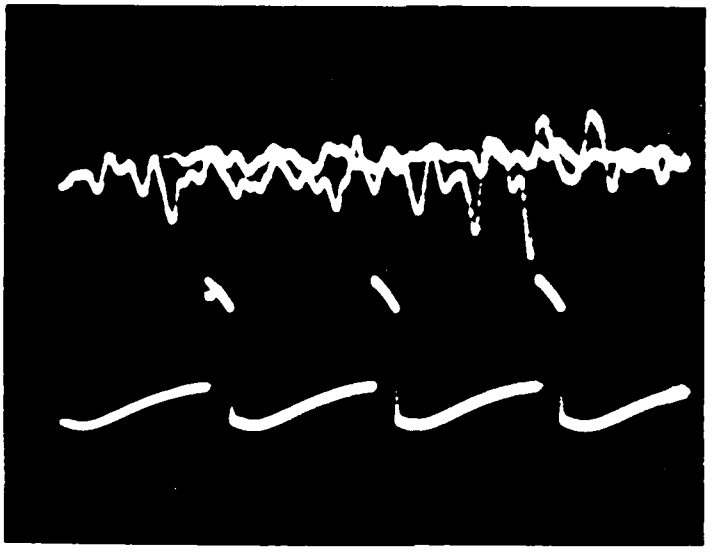

Fig 26. Spanwise Influence of Ribbon at z = -30 mm. Free Stream Velocity: 8.2 m/s; Model 4; Input to Ribbon 6: 71.4 Hz at 6.14 V_{rms}; x_r = 25 mm; $y_r \approx 0$ mm; x_a = 51 mm; y_a = 0.75 mm

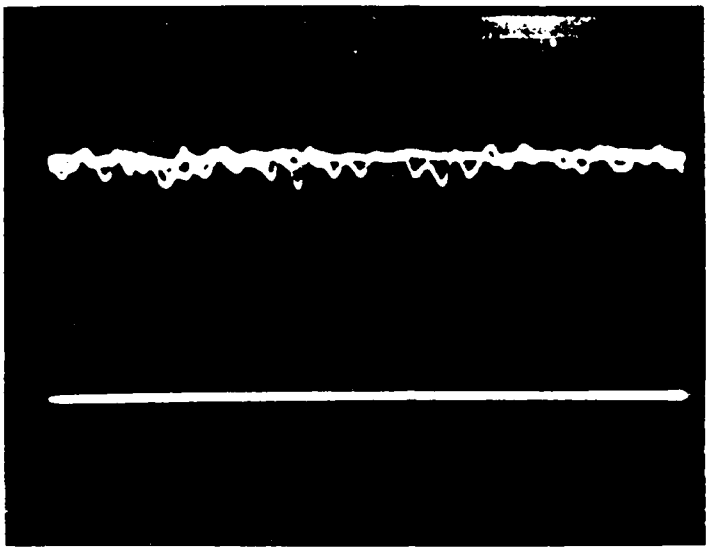

Fig 27. Spanwise Influence of Ribbon at z = -30 mm with No Input to Ribbon 6. Free Stream Velocity: 8.2 m/s; Model 4; x_r = 25 mm; $y_r \approx$ 0 mm; x_a = 51 mm; y_a = 0.75 mm

The maximum turbulence intensity levels u^+_{max}/U_∞ were obtained along a 100 mm spanwise section of the model. Table VI show the wide variation in the amplitude of the disturbances generated along the vibrating ribbon.

Table VI. Variations in Maximum Boundary Layer Turbulence Across the Ribbon. Ribbon Location: x = 25 mm; Free Stream Velocity: 8.2 m/s; Ribbon Input: 71.4 Hz at 6.14 Vrms.

Distance from Centerline (mm)	-50	-40	-30 *	-20	-10 **	0	+10	+20	+30	+40	+50
$u^+_{max}/U_\infty \times 100$	1.2	3.0	6.9	1.2	1.0	1.3	1.1	1.7	6.5	4.9	4.6

* Figure 26
** Figure 25

The large variations in Table VI are primarily caused by non-uniformities in the placement of the ribbon on the model surface. The spring tension system used in these experiments was placed on the underside of the model. The Nichrome ribbon was wrapped around the edges of the model and pulled taut from a location beneath the model. Crimping of the ribbon as it passed over the sides of the model prohibited the ribbon tension system from taking up the slack as the ribbon expanded during heating. As the ribbon expanded, isolated areas were forced off the surface of the model. The higher turbulence levels in Table VI were found to occur in areas where the ribbon was furthest from the surface.

A new ribbon traversing mechanism was introduced in an attempt to gain better control of the ribbon vibration. This device illustrated in Fig 8(b), applies the tension directly in-line with the ribbon. This device eliminated the crimping problem and improved the uniformity of the disturbances generated by the ribbon. Figure 28 shows the spanwise variation in the boundary layer disturbances due to the vibrating ribbon. Trace (a) shows the sinusoidal disturbance generated in the boundary layer 35 mm from the centerline. Toward the center of the model, trace (b), the disturbance amplitude decreased slightly but maintained the same frequency and phase characteristics. At the centerline, trace (c), the disturbance shows a 180 deg shift in phase. At a position 20 mm on the other side of the

centerline, trace (d), the disturbance appears identical to that generated at the centerline. The disturbance shown in trace (e) has the same frequncy characteristics; however, the disturbance amplitude was greatly reduced. These five traces demonstrate the ability to produce a more uniform disturbance using the new ribbon traversing mechanism. The phase and amplitude changes across the span indicate the presence of vibration nodes and some of the remaining non-uniform aspects of the ribbon vibration.

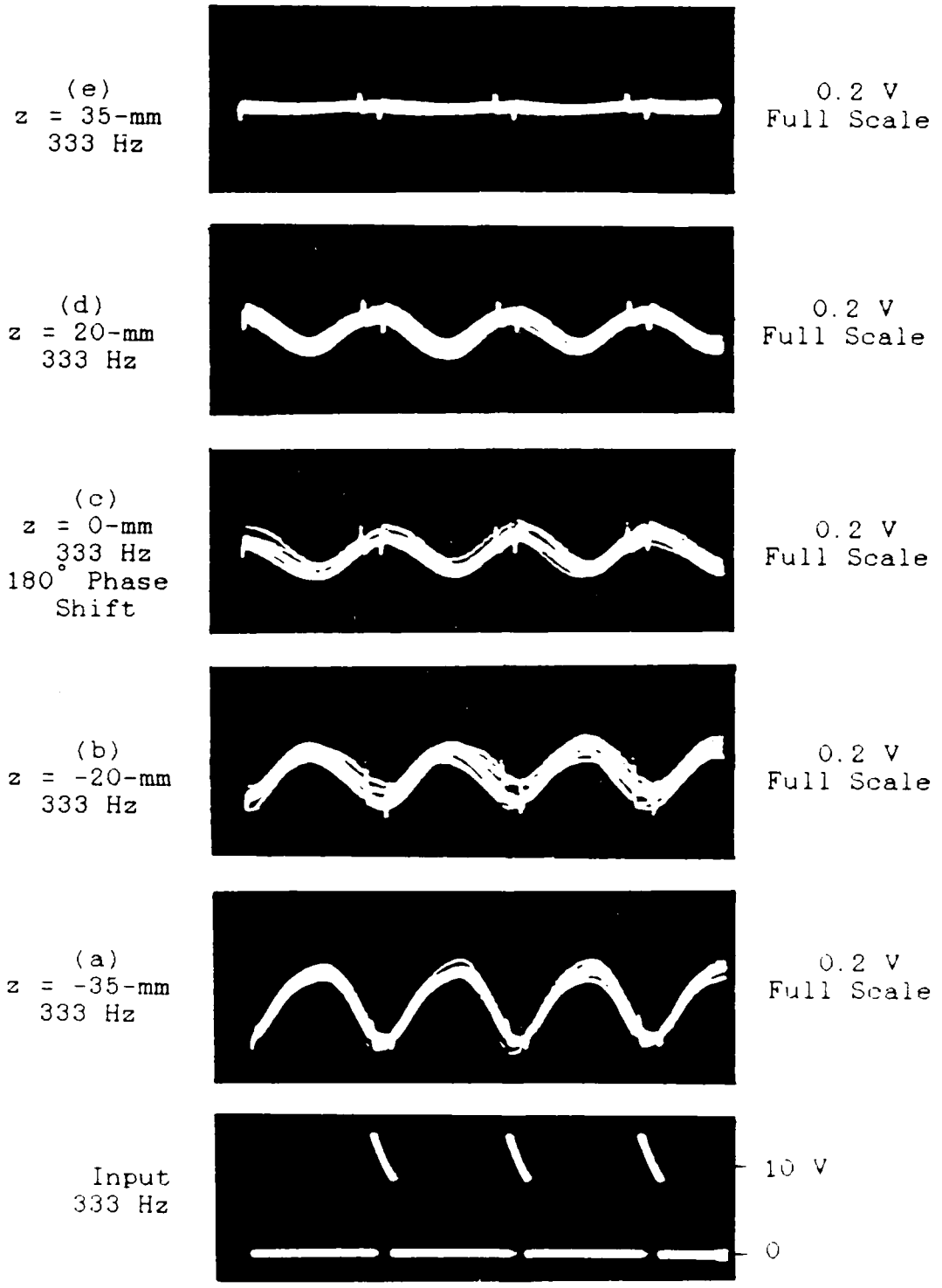

Fig 28. Influence of the Ribbon Across the Span of Model 6. Free Stream Velocity: 11.6 m/s; Input: 333 Hz at 3.75 V_{rms}; x_r = 127 mm; $y_r \approx 0$ mm; x_a = 159 mm; y_a = 1 mm

In subsequent experiments, the influence of a vibrating ribbon, placed entirely outside of the boundary layer (y_r= 8.4 mm), was investigated. Periodic velocity disturbances, related to the ribbon input frequency, were detected by the anemometer probe placed directly behind the ribbon. However, as the probe was lowered into the boundary layer, these periodic disturbances disappeared. The ribbon was then placed inside the boundary layer at: x_r= 127 mm and y_r= 2.2 mm. Figure 29 shows how the boundary layer responded 19 mm downstream of the ribbon. Traces (a) and (b) exhibit the same frequency and amplitude characteristics. There is a 180 deg shift in the phase of the disturbance somewhere between y_a= 2.2 mm and y_a= 3.2 mm. The amplitude of the oscillations approaches zero at the point in the boundary layer were this shift occurs. As the boundary layer probe was moved closer to the wall, the oscillations produced by the ribbon began to diminish. Trace (c) shows that at a distance y_a= 1 mm from the wall the disturbance is no longer evident. These three traces indicated that the position of the ribbon in the boundary layer influences: 1) where the maximum amplitude disturbances will be created, and 2) the location at which the created disturbance will undergo a shift in phase.

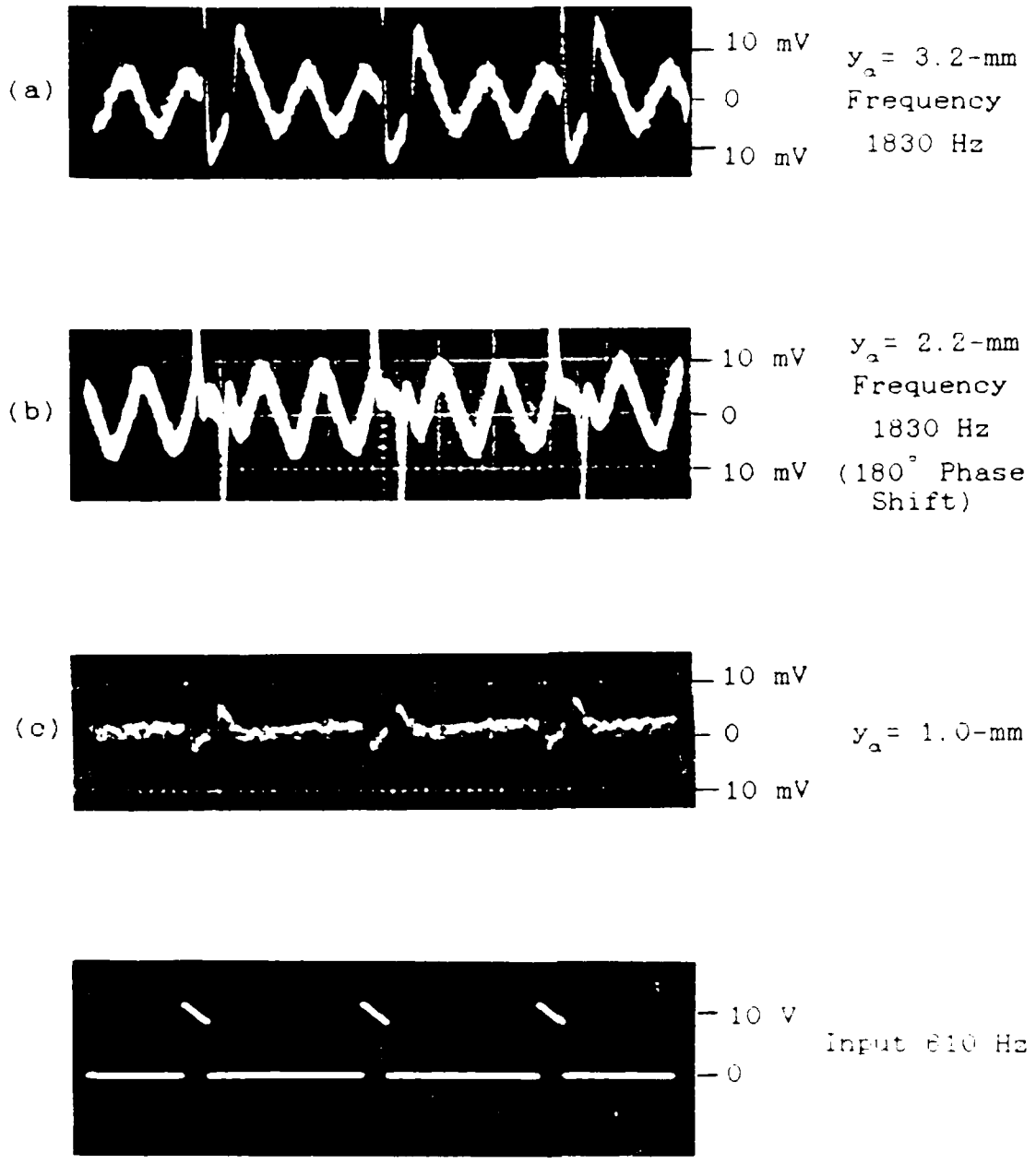

Fig 29. Boundary Layer Response to a Ribbon Placed in the Boundary Layer 2.2 mm Above the Model Surface. Free Stream Velocity: 5.7 m/s; Model 6; Input: 610 Hz at 3.33 V_{rms}; x_r = 127 mm; x_a = 146 mm

The influence of the vibration amplitude on boundary layer transition is illustrated in Fig 30. Trace (a) shows a small amplitude disturbance created by the 926 Hz, 3.7 Vrms input to the ribbon. At the dounstream location, x_a = 457 mm, the boundary layer remains laminar, having a turbulence intensity of 1.6 percent (trace (b)). Trace (c) shows that a much larger disturbance is created as the result of an 819 Hz, 3.7 Vrms input to the ribbon. The influence of this larger disturbance is seen dowmstream. At x_a = 457 mm, trace (d), the boundary layer shows more than an 8-fold increase in the turbulence intensity over that of trace (b) to 13.8 percent.

The influence of pure heating (no vibration) by the Nichrome ribbon was investigated by gluing Ribbon 8 to the surface of Models 4 and 6. In all experiments the amount of turbulence in the boundary layer remained unchanged as the ribbon was heated. The highest temperature attained by the ribbon was approximately 128°C as indicated by the temperature indicating paints. Heating alone was tried for: 1) ribbon locations x_r = 88.9 and 254 mm; 2) free stream velocities 4.9 to 8.7 m/s; 3) anemometer locations x_a = 165 to 584 mm; and 4) voltage inputs 0 to 4.0 Vrms.

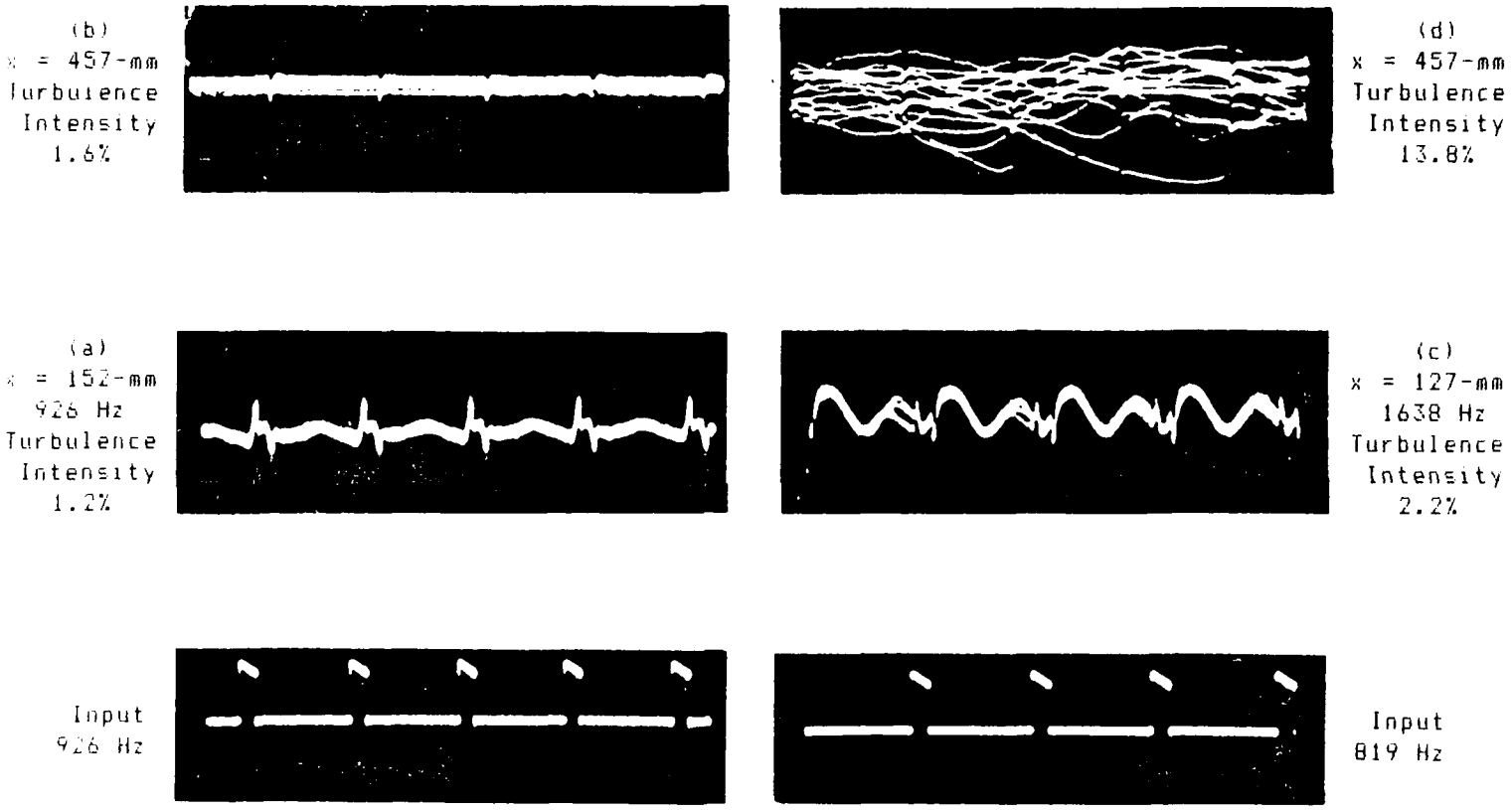

Fig 30. Influence of Initial Disturbance Amplitude on the Turbulence Intensity at 457 mm From the Plate Leading Edge. Free Stream Velocity: 6.3 m/s; Model 6; Input Voltage: 3.7 Vrms; $y_r = 2.0$ mm

VI. Conclusions and Recommendations

Conclusions

The following conclusions are drawn from the experimental result of this thesis:

1. A thin Nichrome ribbon can be made to vibrate by pulsing it with a periodic voltage. The frequency and amplitude of the resulting vibration is influenced by the input voltage and frequency, ribbon tension, and heat transfer environment (i.e., convection and conduction). The ribbon has a resonant mode which can be excited by certain frequency inputs. The frequency of this mode is also influenced by input voltage, ribbon tension, and heat transfer environment.

2. The frequency components, characteristic of the ribbon vibration, are harmonics of the input forcing frequency. For a given input frequency, the amplitudes of the harmonic components change as the ribbon elongates or shortens in response to changes in the input voltage or the amount of heat lost through convection, conduction, etc.

3. Typical mean ribbon temperatures, for a ribbon placed on the surface of a model exposed to an airstream, were 35 to 66 $^{\circ}$C above ambient temperature. During an input cycle, the short voltage pulse followed by a time of cooling resulted in a slight temperature fluctuation (on the order of 1 $^{\circ}$C) about the mean value.

4. The boundary layer oscillations created by the vibrating ribbon have the same frequency composition as the ribbon vibration. The amplitude of the individual frequency compnents changes as the boundary layer develops. The observed downstream amplification and damping of selected frequency components agrees with the predictions of linear stability theory.

5. Placement of the ribbon in the boundary layer (x and y position) influences both the ribbon behavior and the resopnse of the boundary layer to the ribbon. Both, moving the ribbon downstream, and moving it closer to the model surface, result in decreasing the convective heat loss. This raises the mean ribbon temperature. The position of the ribbon in the y-direction determines where the maximum and minimum amplitudes of the created disturbances will be located. At the minimum point the oscillation undergoes a shift in phase of 180 degrees.

6. The location of laminar boundary layer transition is influenced by the initial amplitude of the created oscillations. Increasing the initial disturbance amplitude causes the transition point to move upstream. Because shifts in the ribbon vibration amplitude occur when input voltage, input frequency, free stream conditions, tension, etc. change; the transition point can be altered by simply changing one or more of these parameters.

Recommendations

Recommendations for further work in this area are centered around the ability to control the ribbon vibration.

To improve the controllability of the ribbon, additional information must be obtained on the interaction between the ribbon and its environment (heat transfer, aerodynamic, etc.). Direct correlations between the desired vibration response (frequency, amplitude, and phase characteristics) and external influences (voltage input, free stream velocity, and ribbon tension) would greatly enhance the predictability of the response.

A non-intrusive device, such as a high-speed (100 frames/sec) infra-red camera, to provide detailed heating characteristics of the ribbon such as: 1) an accurate measurement of the ribbon temperature, 2) variations in temperature along the ribbon, 3) direct relationships between ribbon temperature and flow velocity and/or position of the ribbon in the boundary layer.

Additional information is needed as to the influence of heating alone on boundary layer stability. A sinusoidal heat input to the boundary layer may be otained by using several heating elements, or Nichrome ribbons, spaced slightly apart along a section of the model. To accomplish this, an amplifier is needed which is powerful enough to provide more than 2 amperes of current to each ribbon.

Appendix A: AFIT 9-Inch Wind Tunnel

The AFIT 9-in Wind Tunnel is an open circuit, suction type, wind tunnel which provides low-speed, low-turbulence flow throughout the test section. The test section is 9 by 9-in square and 36-in long. The ceiling and floor are wood and the opening side panels are plexiglass. Instumentation access ports, 1-1/2-in in diameter, are located every 5 in along the centerline of the test section ceiling. A photograph of the tunnel is given in Fig 31.

The flow velocity through the test section is measured using a 0 to 2-in H_2O pressure transducer. The transducer measures the pressure difference between the total, or ambient, pressure and the static pressure at 4 pressure ports, one located on each wall of the tunnel upstream of the test section. The transducer was calibrated using an inclined water manometer and the wind tunnel calibration curve for cabin dynamic pressure versus manometer reading. The resulting curve, shown in Fig 32, relates the pressure transducer reading in mV to the test section flow velocity in ft/sec.

Flow quality through the test section was measured in terms of free stream turbulence level u^+/U_∞ and uniformity of velocity profile. The turbulence level and velocity profiles are given in Figs 33 and 34.

Flat plate models 1 thru 3 were mounted in the wind tunnel using a large aluminum support. The influence of the

support blockage beneath Model 2 (8-in wide plate) is illustrated in Fig 35. This figure shows the dramatic changes in the pressure gradient over the model surface. Model 3, which completely spans the 9-in wide test section, has a much more uniform pressure distribution over the surface. The velocity profiles over Model 3, shown in Figs 36, 37, and 38, closely resemble the Blasius boundary layer profiles for a flat plate.

During early boundary layer experiments, the anemometer probe detected small sinusoidal disturbances in the range of 30-120 Hz. (Fig 39). The frequency of these disturbances was directly related to the wind tunnel flow velocity, or motor rpm. The relationship between the disturbances and motor vibration was confirmed using an accelerometer attached to the motor section. Figure 40 shows the linear variation between flow velocity and motor vibration frequency. This figure also indicates the relative vibration amplitude as a function of flow velocity.

The vibration problem was solved by isolating the motor from the upstream test section. The flexible connector shown in Fig 41 was constructed of heavy paper, folded in an accordian type fashion, and taped between the two separated wind tunnel sections. The low frequency disturbances, 30-120 Hz, were eliminated by this connector; however, very small higher frequency signals were still being sensed by the anemometer. These were exactly six times the motor vibration frequency and thought to be acoustic disturbances

generated by the blade-stator interaction of the 6-bladed motor. These small disturbances are consistantly seen in the spectrum analyzer data. The frequency is determined from the free stream velocity.

Fig 31. Photograph of AFIT 9-Inch Wind Tunnel.

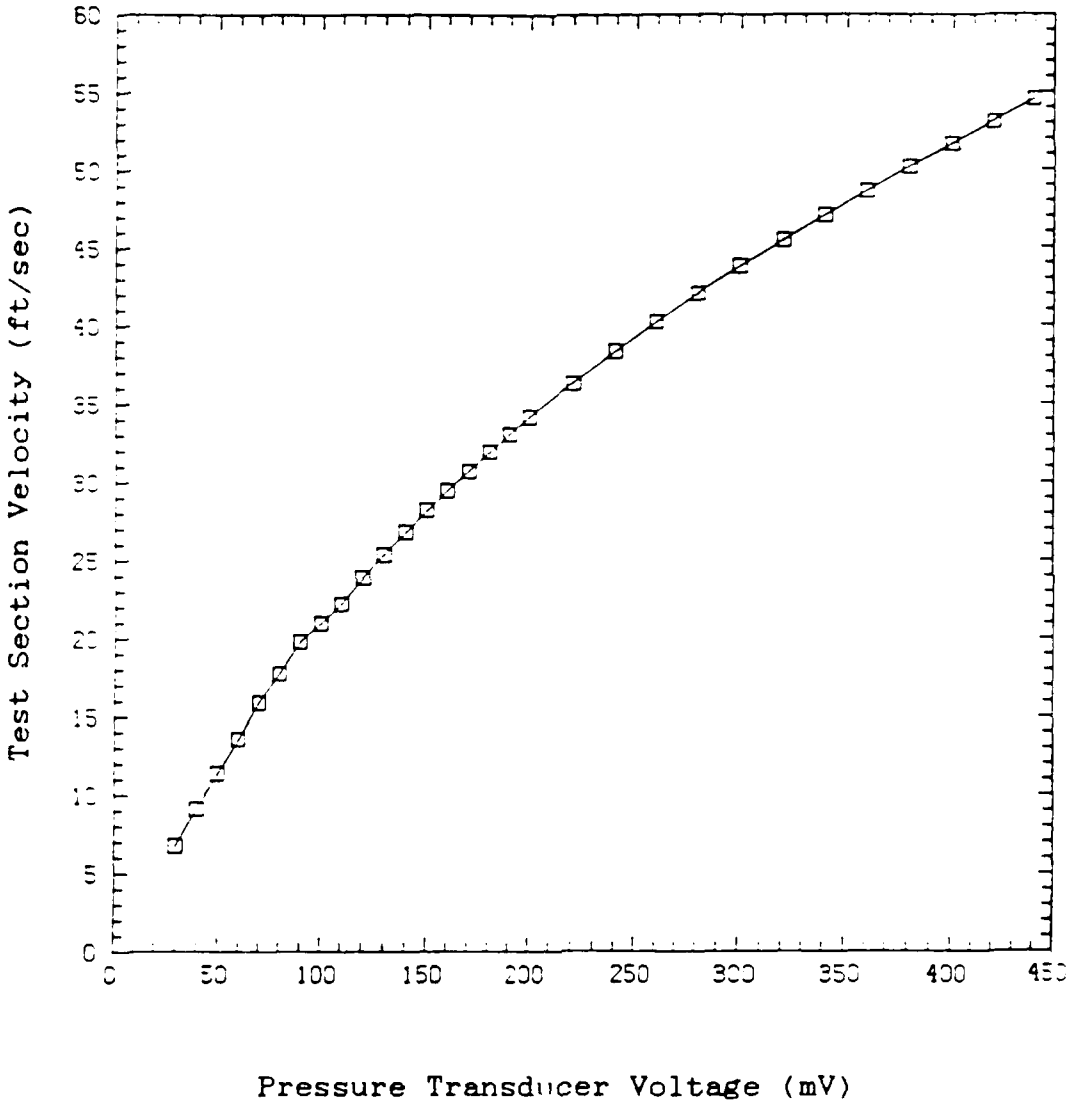

Fig 32. Pressure Transducer Calibration Curve.

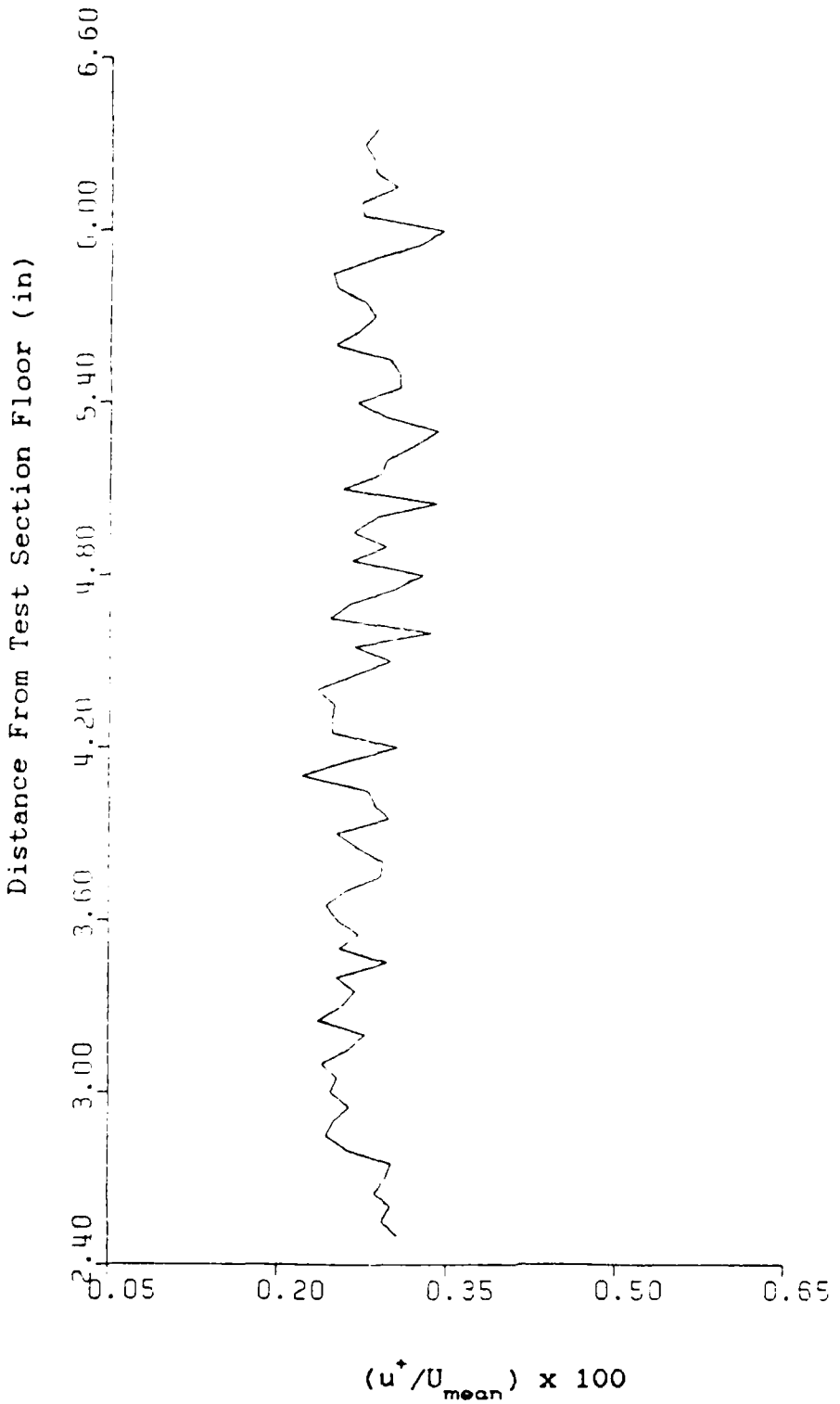

Fig 33. AFIT 9-Inch Wind Tunnel Turbulence Level.
Free Stream Velocity: 26.8 ft/sec

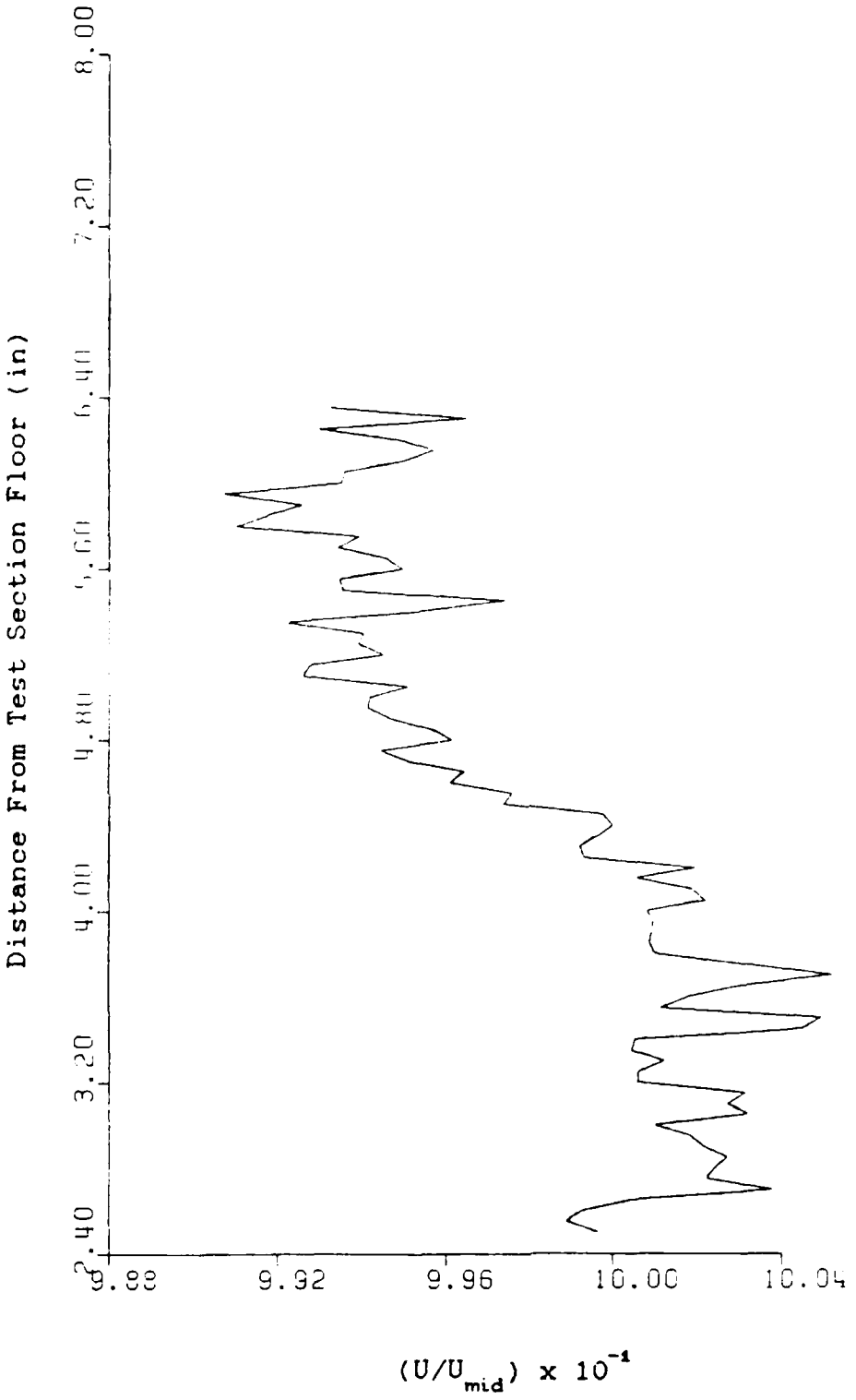

Fig 34. AFIT 9-Inch Wind Tunnel Test Section Velocity Profile. Free Stream Velocity: 26.8 ft/sec

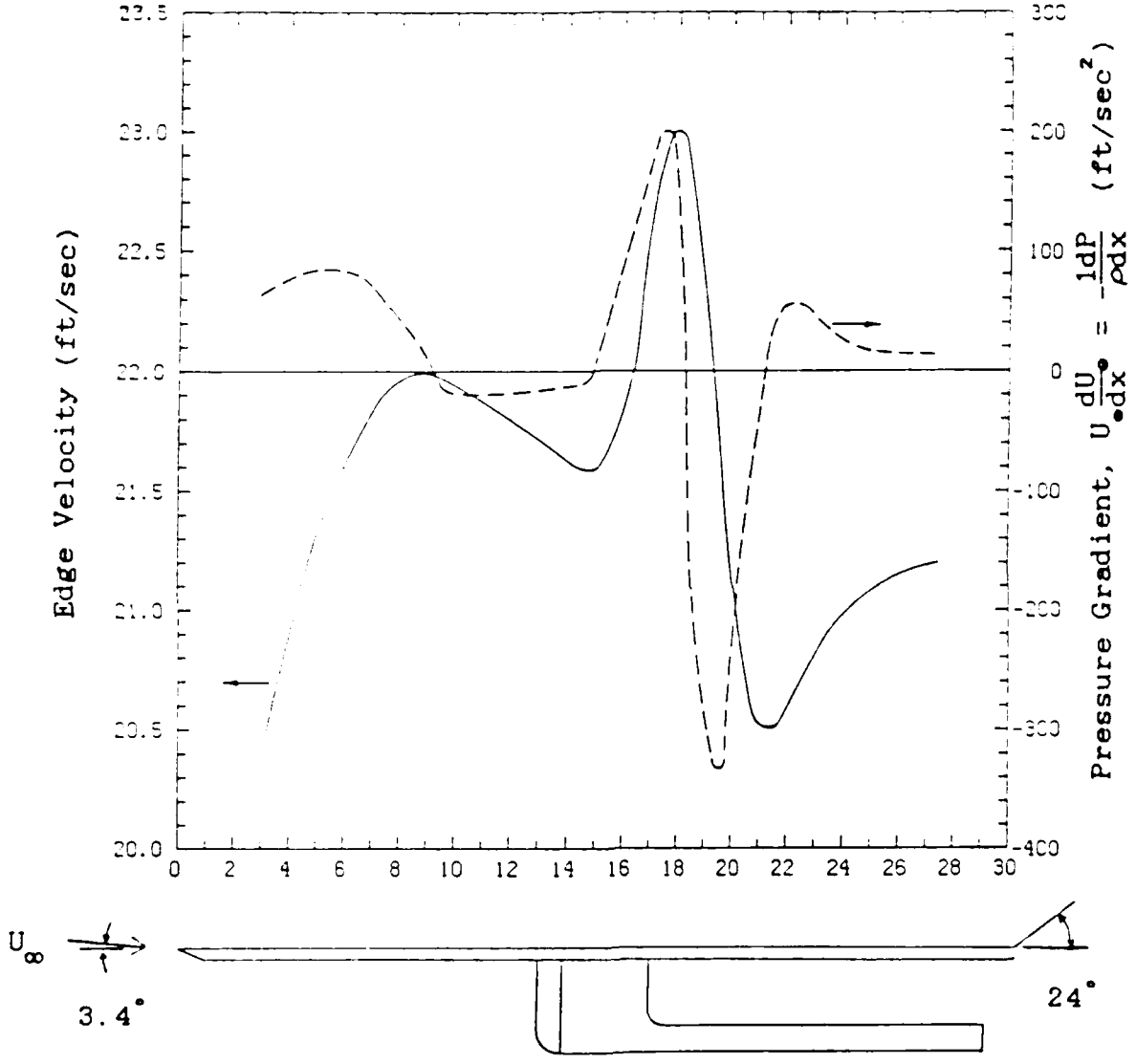

Distance From Leading Edge, x (in)

Fig 35. Edge Velocity and Pressure Gradient over Model 2.

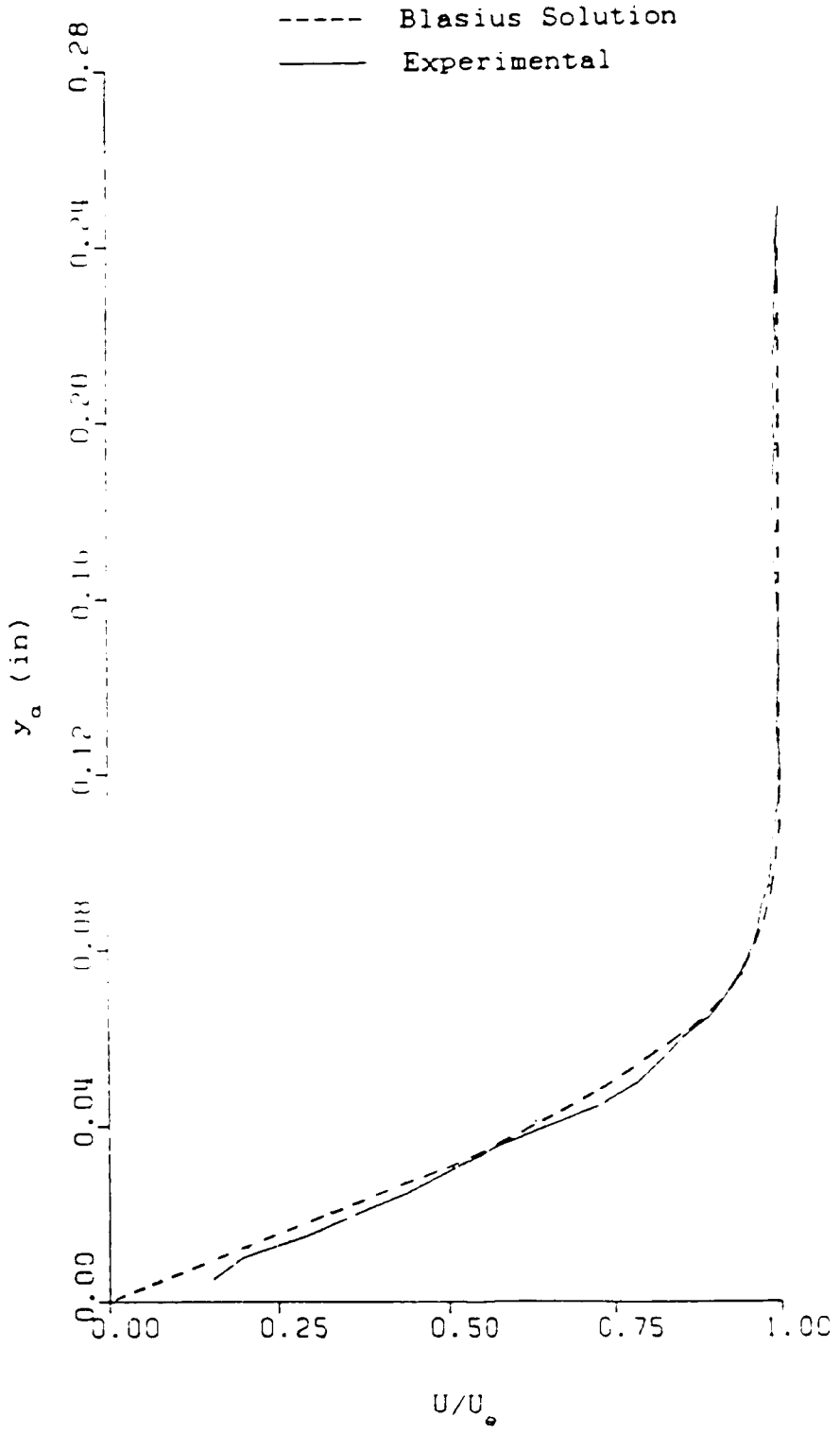

Fig 36. Experimental and Blasius Solution Boundary Layer Profiles over Model 3 at x_a = 5 in. Free Stream Velocity: 23.7 ft/sec

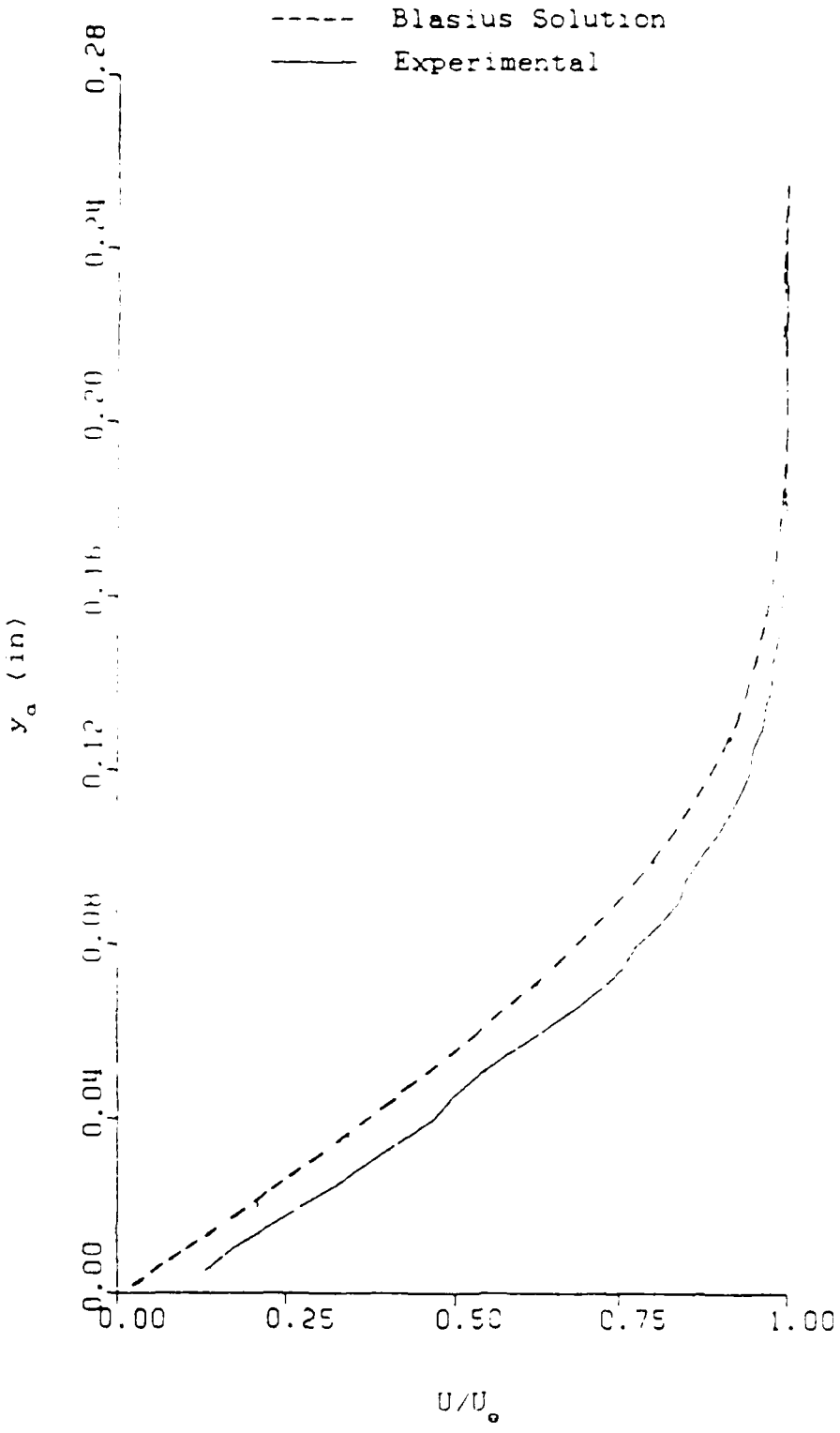

Fig 37. Experimental and Blasius Solution Boundary Layer Profiles over Model 3 at x_o = 15 in. Free Stream Velocity: 23.7 ft/sec

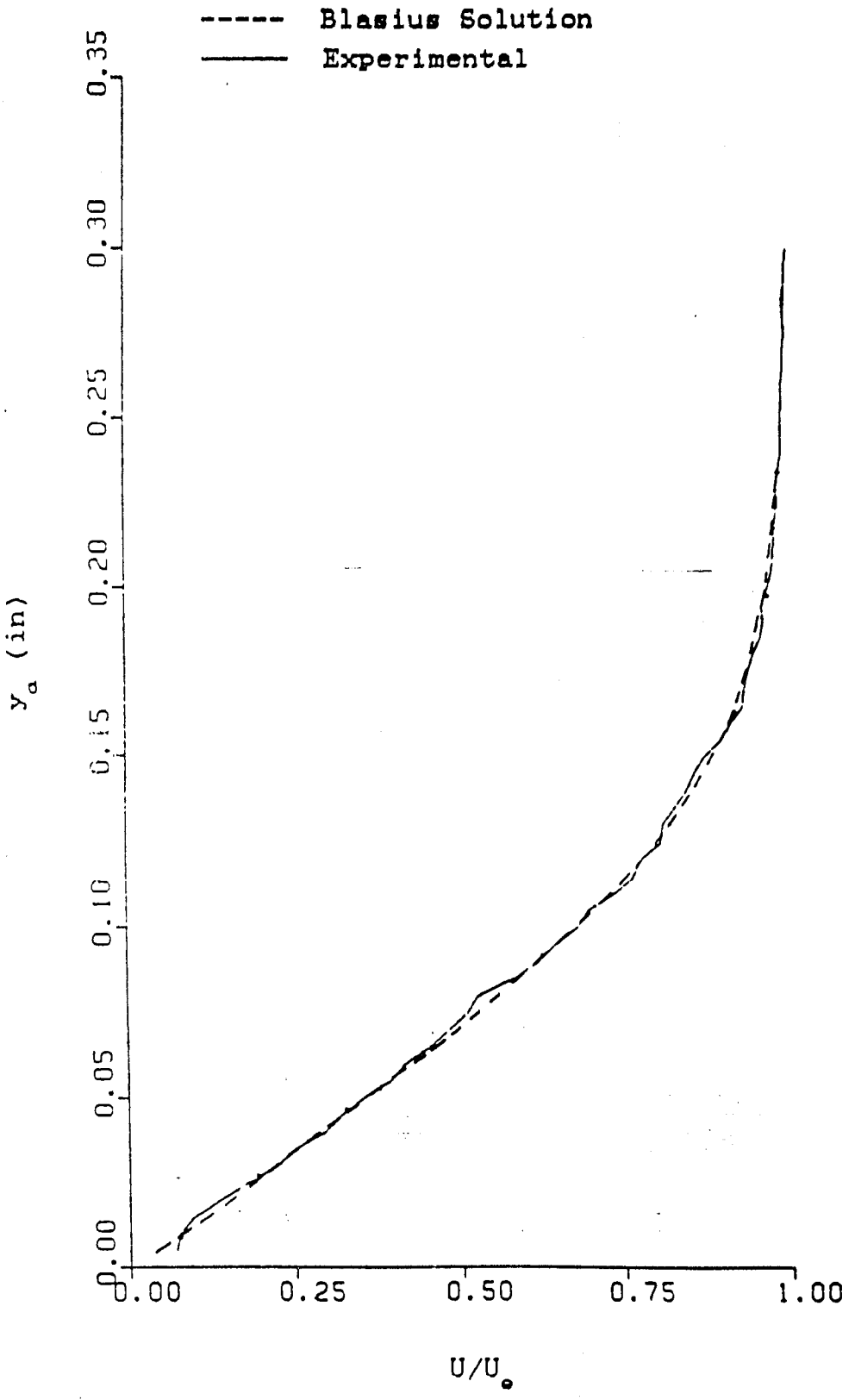

Fig 38. Experimental and Blasius Solution Boundary Layer Profiles over Model 3 at x_a = 25 in. Free Stream Velocity: 23.7 ft/sec

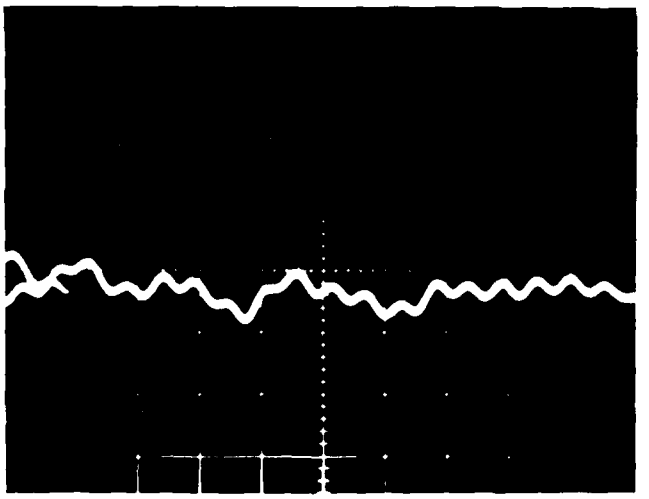

Anemometer
Output
(50mV/div)

Time (2msec/div)

Fig 39. Wind Tunnel Vibration Detected by the Hot Wire Anemometer Probe. Free Stream Velocity: 32 ft/sec; x_a = 6 in; y_a = 0.005 in

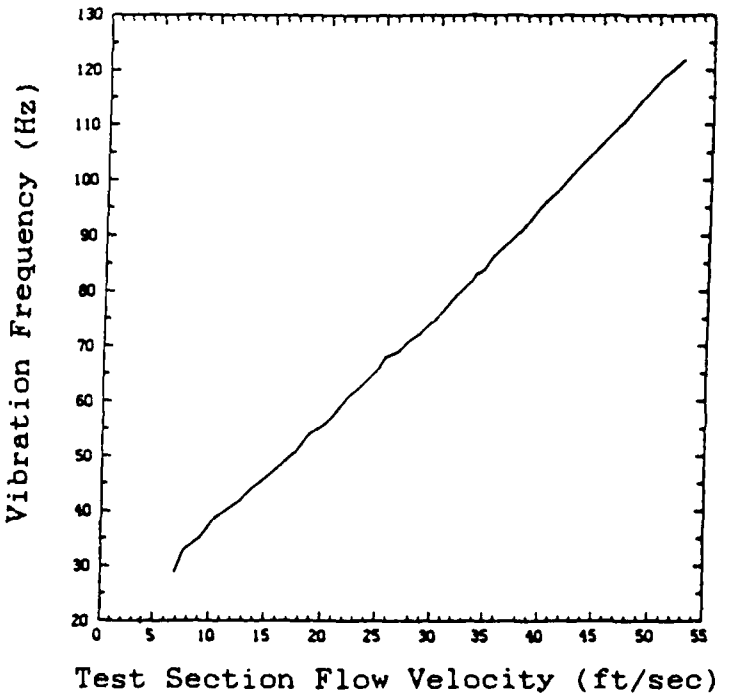

Fig 40. Plot of Wind Tunnel Vibration Frequency versus Test Section Flow Velocity. (Accelerometer data)

Fig 41. Photograph of Flexible Connector used to Isolate Motor Vibration.

Appendix B: VKI L-2A Wind Tunnel

The L-2A Wind Tunnel is located at the von Karman Institute for Fluid Dynamics in Belgium. The facility is an open circuit, low-speed, low-turbulence, suction type wind tunnel. The octagonal test section is 0.28-m wide and 1.30-m long. Modular plexiglass walls make up the two vertical sides and bottom of the test section. The top is covered by a large plexiglass plate 1.23 by 0.62-m. A 1.08 m longitudinal slot was cut in the plate to allow for streamwise mobility of the traversing mechanism. The slot was sealed using tape to prevent leakage. The entire top plate could also be moved in the transverse direction, providing a three-directional traversing capability. Four fixed wood corner sections supported the test section. A photograph of the wind tunnel is shown in Fig 42.

The quality of flow through the test section was measured using a hot wire anemometer. The anemometer was placed in the center of the test section then traversed vertically from -65 mm to +65 mm. The turbulence intensity u^{+}/U_{∞} for free stream velocities 12.8 to 30.0 m/s was uniform across the midsection of the tunnel and differed slightly depending upon free stream velocity (0.48 to 0.52 percent). The velocity profile was also uniform across the test section.

Flat plate Models 4 thru 6 were mounted directly to the plexiglass side walls as shown in Fig 43. This configuration minimized tunnel blockage by eliminating the

presence of a support. It also completely separated flow over the top and bottom of the model. The finite thickness of the models caused the flow to become turbulent over the model surface. This condition was overcome by using a flap attached to the trailing edge of the model. The 76.2 mm variable flap was used to adjust the oncoming streamlines so the stagnation region would lie entirely on the underside of the model. Fig 44 shows the influence the flap angle had on the transition point of the boundary layer. The pressure gradient over Models 4 thru 6 closely resembled flat plate conditions. A zero pressure gradient region was established on these models beginning 0.2 m from the leading edge to about 0.12 m from the trailing edge. The slight favorable pressure gradient near the leading edge and unfavorable pressure gradient near the trailing edge were the direct result of the flap.

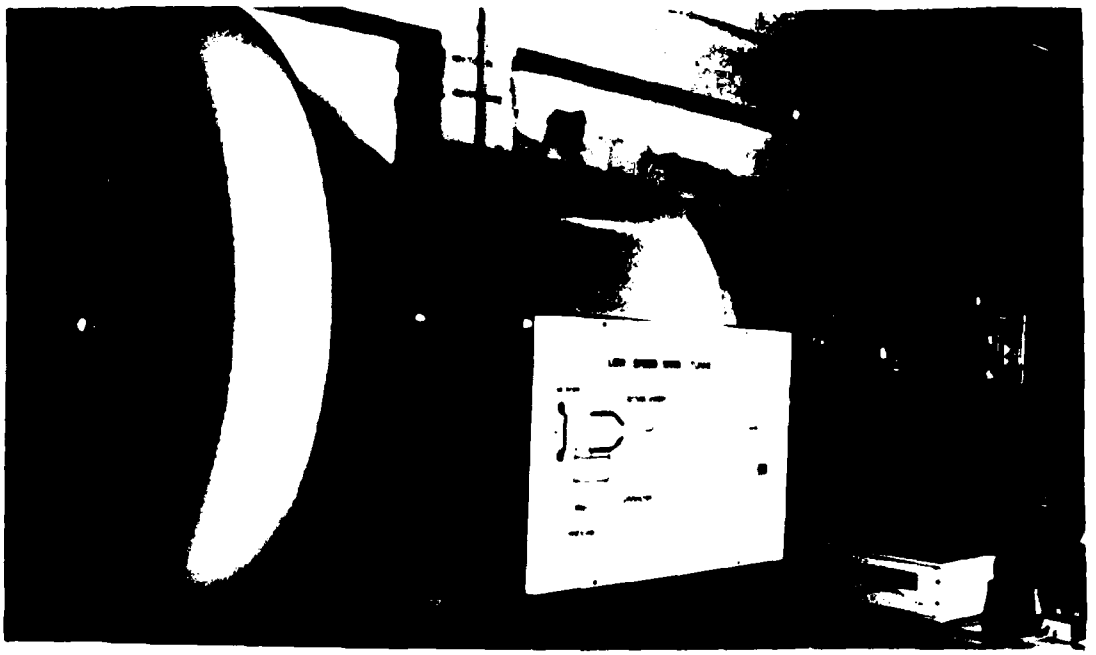

Fig 42. Photograph of VKI L-2A Wind Tunnel.

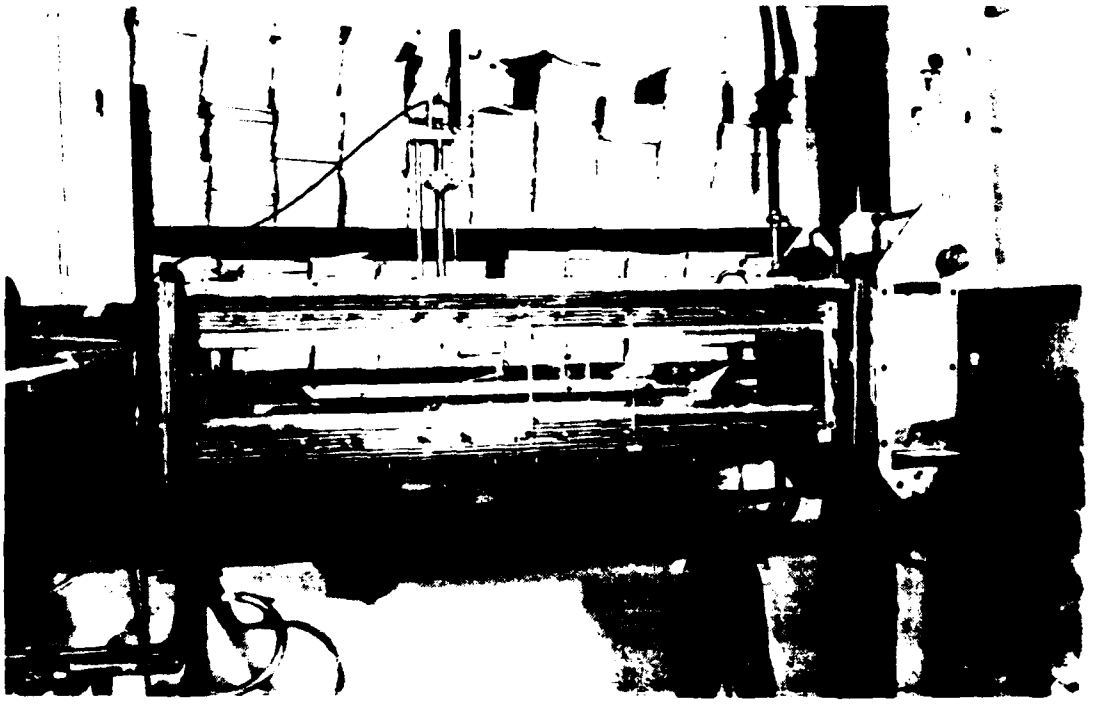

Fig 43. Photograph of L-2A Wind Tunnel Test Section.

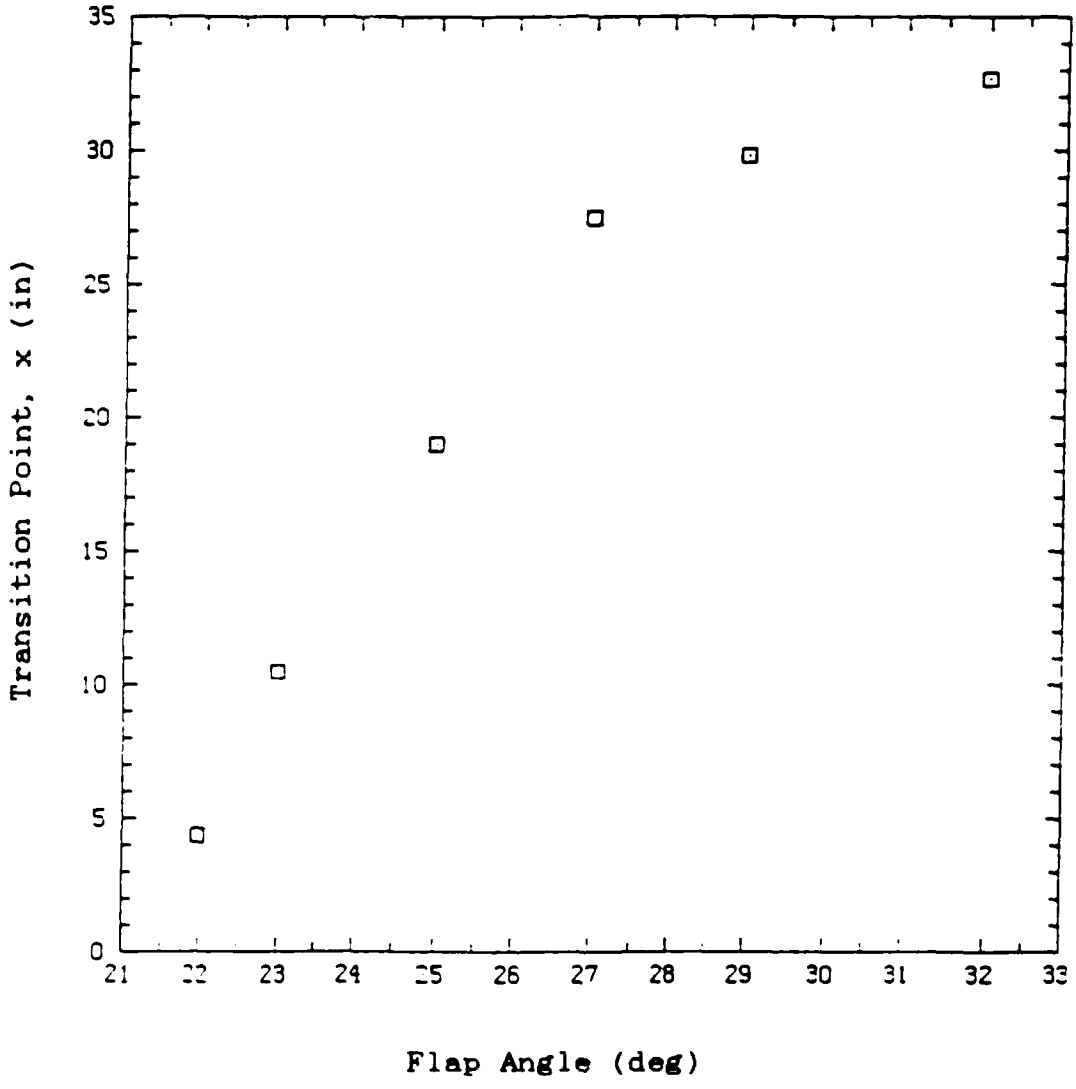

Fig 44. Influence of Flap Angle on Transition Point for Model 5.

Appendix C: Instrumentation List

The instrumentation used at AFIT and the VKI is broken down into three main catagories: 1) Ribbon Control, 2) Ribbon Response, and 3) Boundary Layer. The ribbon control equipment generated the input to the ribbon, then monitored the frequency and voltage of that input. The ribbon response equipment determined the ribbon vibration, heating, and time constant characteristics. The equipment used during the boundary layer experiments supports the hot wire anemometry system in obtaining velocity profiles, turbulence levels, and the nature of the ribbon induced disturbances.

The following is a list of instrumentation used to carry out the experiments of this thesis. Photographs of the instrumentation arrangements at the AFIT and VKI facilities are given in Figs 45 and 46.

I. Ribbon Control

AFIT

a. Hewlett-Packard (HP) 3312A Function Generator
b. Bogen Model C 60B Power Amplifier or Pioneer SA-5800 Stereo Amplifier: 0 to 10 V
c. Eldorado Model 1607 Frequency Counter/Timer
d. HP 3438A Digital Voltmeter

VKI

a. HP 3312A Function Generator
b. Bogen Model C 60B Power Amplifier: 0 to 10 V or Transistor + 6A/30V Bremic Model BRS 33 DC Power Supply: Capable of frequencies > 300 Hz, Voltage < 5 V_{rms} (used after Bogen Amplifier broke)
c. Keithley 177 Microvlot DMM Voltmeter
d. Philips PM 3215 50MHz Dual Channel Oscilloscope

II. Ribbon Response

AFIT(Vibration)

a. Mechanical Technology Inc. KD-320 Fotonic Sensor
b. HP 3582A Low Frequency Spectrum Analyzer
c. B-K Precision Dual Time Base Oscilloscope
d. Tektronix Model C-30 Series Camera

VKI(Heating and Time Constant)

a. Thermindex Temperature Indicating Labels 43°C - 204°C
b. Tempilaq Temperature Indicating Paint: 38, 52, 69, and 128°C
c. Copper-Constantan Thermocouple 0.2 mm dia
d. Enregistreur Asservi Gravispot type GRVAT No. 1435 Time Based Plotter
e. Strain Gage Balance 0 - 500g
f. Transducer Power Supply for the Strain Gage Balance
g. Keithley 177 Microvolt DMM Voltmeter

III. Boundary Layer

AFIT

a. Thermo Systems Inc.(TSI) IFA-100 Intellegent Flow Analyzer Anemometry System
b. TSI Model 1218-20 Hot Film Boundary Layer Probe
c. Zenith Z-100 Personal Computer with an A-to-D Converter Card to Record Anemometer Output
d. HP 3582A Low Frequency Spectrum Analyzer
e. B-K Precision Dual Time Base Oscilloscpe
f. Tektronix Model C-30 Series Camera
g. Camera Adapter Frames for Oscilloscope and Spectrum Analyzer

VKI

a. VKI Instruments Hot Wire Anemometry System with Linearizer
b. VKI Instruments Hot Wire Boundary Layer Probe
c. Philips PM 3215 50 MHz Dual Channel Oscilloscope
d. Polaroid CU-5 Land Camera
e. Camera Adapter Frame for the Oscilloscope
f. Microcontrol 0.01 mm Traversing Mechanism
g. Lunette-Wild Optical Measurement Device for measuring the distance of the boundary layer probe from the model surface
h. Sakae type 0F20LP100 Displacement Potentiometer

for measuring the y-position of the boundary layer traverse

i. Philips PE 1542 DC Power Supply for the Poteniometer

j. HP Mosely Autograph Model 7001 AM X-Y Recorder

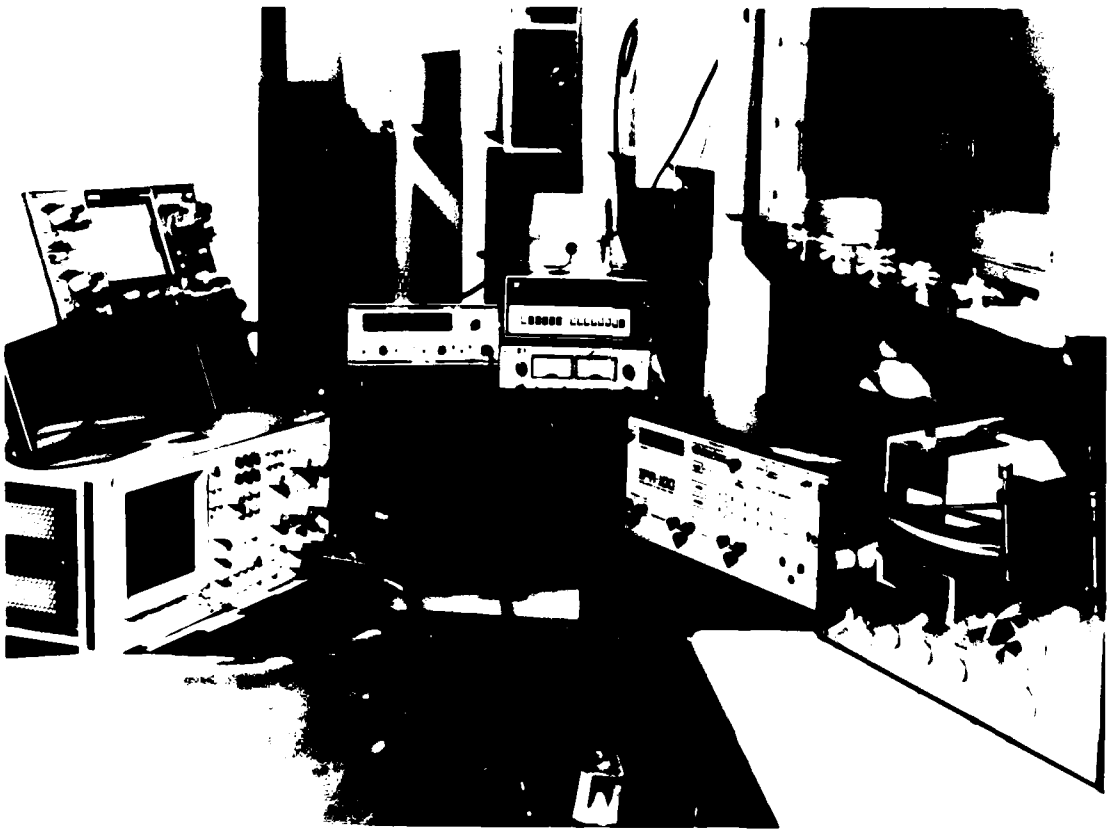

Fig 45. Photograph of AFIT Equipment Arrangement.

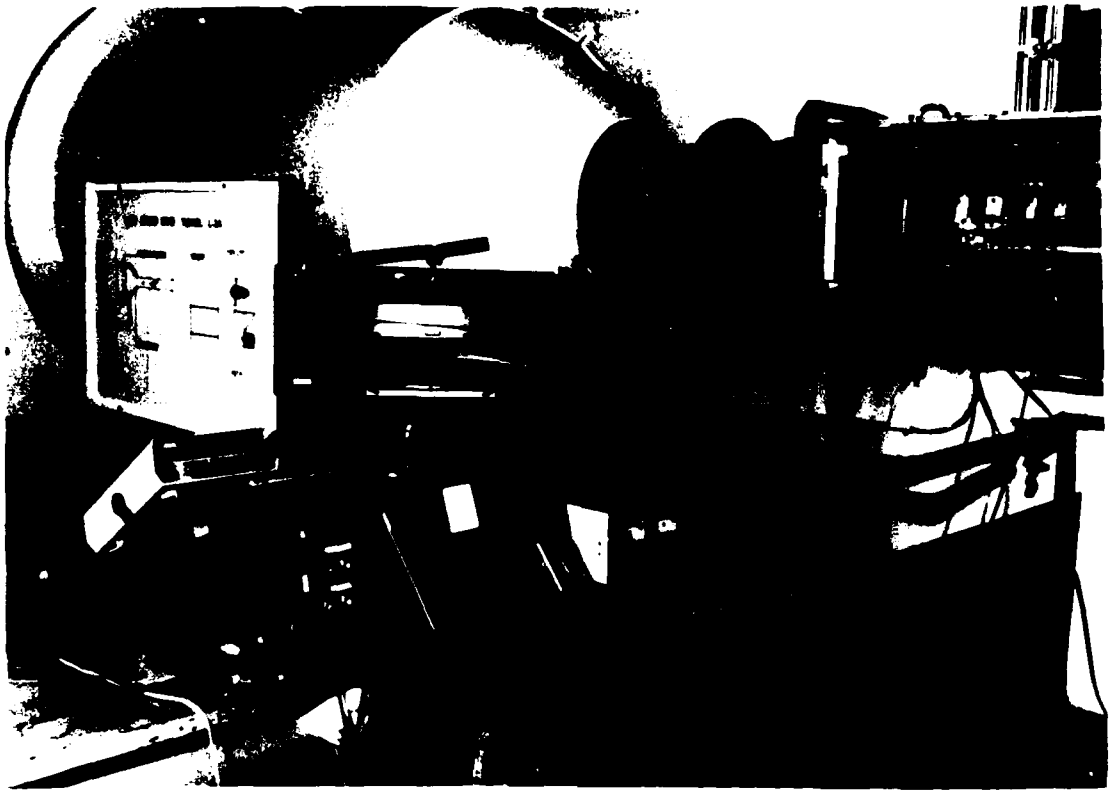

Fig 46. Photograph of VKI Equipment Arrangement.

BIBLIOGRAPHY

1. Arnal, Daniel. "Description and Prediction of Transtion in Two-Dimensional Incompressible Flow", Special Course on Stability and Transition of Laminar Flow, AGARD Report 709, June 1894.

2. Bayliss, A., L. Maestrello P. Parikh, and E. Turkel. "Numerical Simulation of Boundary Layer Excitation by Surface Heating/Cooling", Proceedings of the AIAA Shear Flow Conference. Paper No 85-0565. New York: American Institute of Aeronautics and Astronautics, March 1985.

3. Bird, R.B., W.E. Stewart, and E.N. Lightfoot. Transport Phenomenon. New York: John Wiley & Sons, Inc., 1960.

4. Eckert E.R.G. and R.J. Goldstein. Measurements in Heat Transfer. (Second Edition), Hemisphere Publishing Corp. Washington, New York: McGraw-Hill Book Company, 1976.

5. Gaster, M. "On the Generation of Spacially Growing Waves in a Boundary Layer", Journal of Fluid Mechanics, 22:433-441 (1965).

6. Gedney, C.J. "The Cancellation of a Sound-Excited Tollmien-Schlicting Wave with Plate Vibration, Physics of Fluids, 26:1158-1160 (May 1983).

7. Giliv, V.M. Tollmien-Schlichting Wave Excitation on the Vibrator and Laminar-Turbulent Transition Control", IUTAM Symposium on Laminar-Turbulent Transition, Novosibirsk 1984, Springer-Verlag (1985).

8. Rohsenow, W.P. and J.P. Hartnett, Handbook of Heat Transfer fundamentals. (Second Edition), New York: McGraw-Hill Book Co., 1985.

9. Klebanoff, P.S., K.D. Tidstrom, and L.M. Sargent. "The Three-Dimensional Nature of Boundary Layer Instability", Journal of Fluid Mechanics, Vol 12 Part 1:1-32 (1962).

10. Koshlyakov, N.S., M.M. Smirnov, and E.B. Gliner. Differential Equations of Mathematical Physics. New York: John Wiley and Sons., 1964.

11. Kudelka, Capt Lawrence. Boundary Layer Disturbances Caused by Periodic Heating of A Thin Ribbon. MS Thesis, AFIT/GAE/AA/86D-7. School of Engineering, Air Force Institute of Technology (AU), Wright-Patterson AFB OH, December 1986.

12. Leehey, P., C.J. Gedney, and J.Y. Her. "The Receptivity of a Laminar Boundary Layer to External Disturbances", IUTAM Symposium on Laminar-Turbulent Transition, Novosibirsk 1984, Springer-Verlag (1985).

13. Liepmann, H.W. and D.M. Nosenchuck. "Active Control of Laminar-Turbulent Transition", Journal of Fluid Mechanics, 118:201-204 (1982).

14. Liepmann, H.W., G.L. Brown, and D.M. Nosenchuck. "Control of Laminar Instability Waves Using a New Technique", Journal of Fluid Mechanics, 118:187-200 (1982).

15. Ligrani. Measurement Techniques: Course Note 108, von Karman Institute for Fluid Dynamics, Oct 1979.

16. Mack, Leslie M. "Boundary Layer Linear Stability Theory", Special Course on Stability and Transition of Laminar Flow, AGARD Report 709, June 1984.

17. Maestrello, Lucio. "Active Transition Fixing and Control of the Boundary Layer in Air", Proceedings of the AIAA Shear Flow Conference. Paper No 85-0564, New York: American Institute of Aeronautics and Astronautics, January 1984.

18. Maestrello, Lucio and Lu Ting. "Analysis of Active Control by Surface Heating", Proceedings of the AIAA 22nd Aerospace Science Meeting. Paper No. 84-0173, New York: American Institute of Aeronautics and Astronautics, January 1984.

19. Nosenchuck, D.M., M.K. Lynch, and J.P. Stratton. "Active Control of Sublayer Disturbances Using and Array of Heating Elements", Proceedings of the ASME-JSME Thermal Engineering Joint Conference, 619-627. Honolulu, Hawaii, March 1987.

20. Pender, H., and W.A. Del Mar. Electrical Engineers' Handbook Electric Power. (Fourth Edition), New York: Wiley Engineerig Handbook series, 1958.

21. Reshotko, E. "Environment and Receptivity", Special Course of Stability and Transition of Laminar Flow, AGARD Report 709, June 1984.

22. Schlichting, Herman W. Boundary Layer Theory. (Seventh Edition), New York: McGraw-Hill Book Co., 1979.

23. Schubauer, G.B. and H.K. Skramstad. "Laminar Boundary-Layer Oscillations and Stability of Laminar Flow", Journal of the Aeronautical Sciences, 14:69-78 (February 1947).

24. Thomas, Andrew S.W. "The Control of Boundary-Layer Transition Using a Wave-Superposition Principle", Journal of Fluid Mechanics, 137:233-250 (1983).

25. Wylie, Ray C. and Louis C. Barrett. Advanced Engineering Mathematics, (Fifth Edition), New York: McGraw-Hill Book Company, 1982.

Vita

Captain Brenda Haven was born [redacted] She graduated from Ashwaubenon High School, [redacted] PII Redacted Green Bay, Wisconsin, in 1979 and attended the University of Minnesota, Minneapolis, where she earned the degree of Bachelor of Science in Aerospace Engineering in June of 1983. Upon graduation, she received a commission in the USAF through the ROTC program and was assigned to Wright-Patterson AFB where she worked as a Flight Systems Engineer until entering the School of Engineering, Air Force Institute of Technology, in June of 1986.

UNCLASSIFIED

SECURITY CLASSIFICATION OF THIS PAGE

REPORT DOCUMENTATION PAGE

Form Approved OMB No. 0704-0188

1a. REPORT SECURITY CLASSIFICATION: UNCLASSIFIED	1b. RESTRICTIVE MARKINGS: None
2a. SECURITY CLASSIFICATION AUTHORITY	3. DISTRIBUTION/AVAILABILITY OF REPORT: Approved for public release; distribution unlimited.
2b. DECLASSIFICATION/DOWNGRADING SCHEDULE	
4. PERFORMING ORGANIZATION REPORT NUMBER(S): AFIT/GAE/AA/88M-2	5. MONITORING ORGANIZATION REPORT NUMBER(S)
6a. NAME OF PERFORMING ORGANIZATION: School of Engineering; 6b. OFFICE SYMBOL (*If applicable*): AFIT/ENY	7a. NAME OF MONITORING ORGANIZATION
6c. ADDRESS (*City, State, and ZIP Code*): Air Force Institute of Technology, Wright-Patterson AFB, OH 45433-6583	7b. ADDRESS (*City, State, and ZIP Code*)
8a. NAME OF FUNDING/SPONSORING ORGANIZATION: Structural Vibration Br. Flight Dynamics Lab.; 8b. OFFICE SYMBOL (*If applicable*): AFWAL/FIBG	9. PROCUREMENT INSTRUMENT IDENTIFICATION NUMBER
8c. ADDRESS (*City, State, and ZIP Code*): AFWAL/FIBG, Wright-Patterson AFB, OH 45433	10. SOURCE OF FUNDING NUMBERS: PROGRAM ELEMENT NO. / PROJECT NO / TASK NO / WORK UNIT ACCESSION NO.

11. TITLE (*Include Security Classification*): See box 19 UNCLASSIFIED

12. PERSONAL AUTHOR(S): Brenda A. Haven, B.S., Capt, USAF

13a. TYPE OF REPORT	13b. TIME COVERED	14. DATE OF REPORT (*Year, Month, Day*)	15. PAGE COUNT
MS Thesis	FROM _____ TO _____	1988 March	109

16. SUPPLEMENTARY NOTATION

17. COSATI CODES			18. SUBJECT TERMS (*Continue on reverse if necessary and identify by block number*)
FIELD	GROUP	SUB-GROUP	Boundary Layer Transition Laminar Boundary Layer
01	03		
20	04		

19. ABSTRACT (*Continue on reverse if necessary and identify by block number*)

Title: INVESTIGATION OF BOUNDARY LAYER DISTURBANCES CAUSED BY PERIODIC HEATING OF A THIN RIBBON

Thesis Advisor: Milton E. Franke, PhD
Professor of Aerospace Engineering

Approved for public release: IAW AFR 190-1.
21 Mar 88
Dean for Research and Development
Air Force Institute of Technology
Wright-Patterson AFB OH 45433

20. DISTRIBUTION/AVAILABILITY OF ABSTRACT	21. ABSTRACT SECURITY CLASSIFICATION
☐ UNCLASSIFIED/UNLIMITED ☒ SAME AS RPT ☐ DTIC USERS	UNCLASSIFIED

22a. NAME OF RESPONSIBLE INDIVIDUAL	22b. TELEPHONE (*Include Area Code*)	22c. OFFICE SYMBOL
Milton E. Franke, Professor	513-255-2362	AFIT/ENY

DD Form 1473, JUN 86 *Previous editions are obsolete.*

SECURITY CLASSIFICATION OF THIS PAGE

UNCLASSIFIED

Abstract

Wind tunnel experiments were conducted to investigate the use of a periodically heated Nichrome ribbon as a boundary layer control device. The specific items of interest were: 1) the physical parameters governing the ribbon behavior, 2) the consequence of the ribbon on the downstream development of the laminar boundary layer, and 3) the controllability of the ribbon to produce the desired consequence.

The thin ribbon was placed on or near the surface of 0.76-m and 0.91-m-long, flat plate models. The periodic voltage applied across the ribbon caused it to vibrate at a frequency or frequencies harmonic with the input frequency. The amplitude and frequency composition of the vibration was influenced by input voltage and frequency, applied tension to the ribbon, and flow velocity over the model.

The disturbances detected in the boundary layer immediately downstream of the vibrating ribbon exhibited the same frequency characteristics as the ribbon. The evolution of these disturbances in the boundary layer was studied by positioning a hot wire anemometer, boundary layer probe at different locations behind the ribbon. The selective amplification and damping of the disturbance frequencies agreed with the predictions of linear Tollmien-Schlichting stability theory.

The ribbon vibration could not be controlled to provide a specified vibration frequency or amplitude with the control system used in this research. Boundary layer control schemes requiring careful selection of a controlling disturbance would be extremely difficult to implement using this technique. Without precise control of the ribbon vibration, unwanted frequencies are introduced into the boundary layer. The interaction of these disturbances was shown to accelerate the laminar to turbulent transition process.